

Supplementary Information

Chromogenic Chemosensors Based on Phenolic Imines for the Detection of Alkylamines and Lidocaine in Water and in the Vapor Phase

*Eduardo A. Ribeiro^{a,b} and Vanderlei G. Machado  ^{*a}*

*^aDepartamento de Química, Universidade Federal de Santa Catarina (UFSC),
88040-900 Florianópolis-SC, Brazil*

^bInstituto Federal de Santa Catarina (IFSC), 88813-600 Criciúma-SC, Brazil

*e-mail: vanderlei.machado@ufsc.br

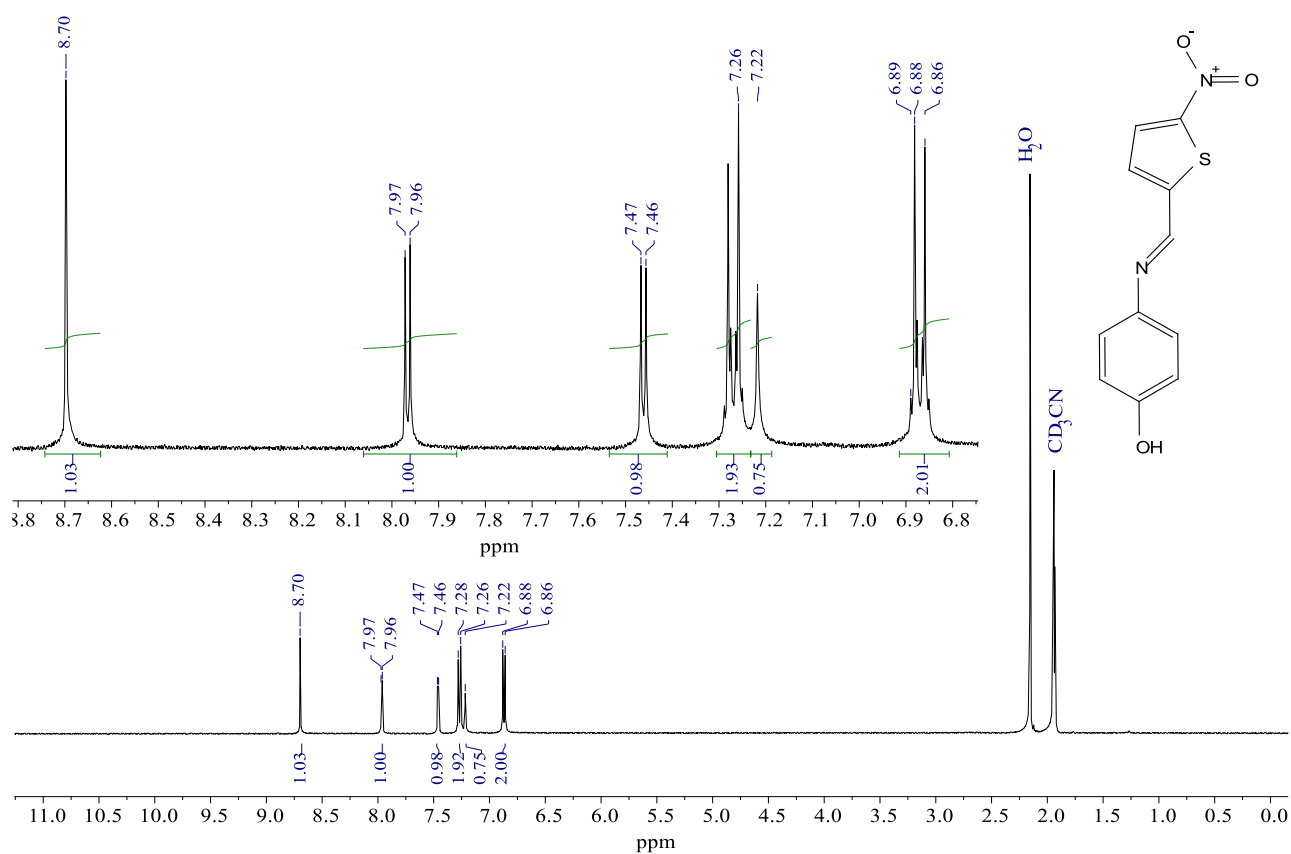


Figure S1. ¹H NMR spectrum (400 MHz, CD₃CN) of compound 3a.

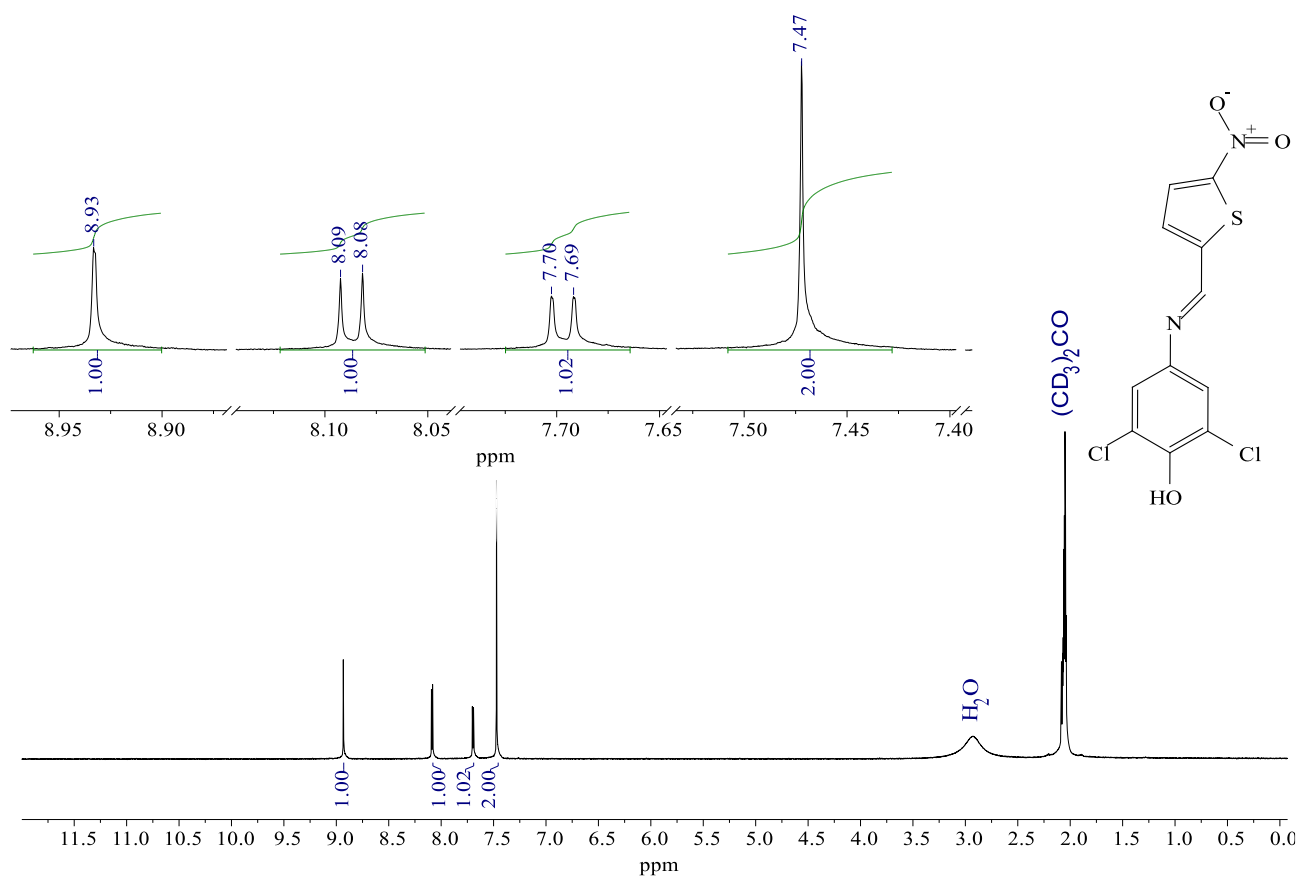


Figure S2. ^1H NMR spectrum (400 MHz, $\text{acetone-}d_6$) of compound **4a**.

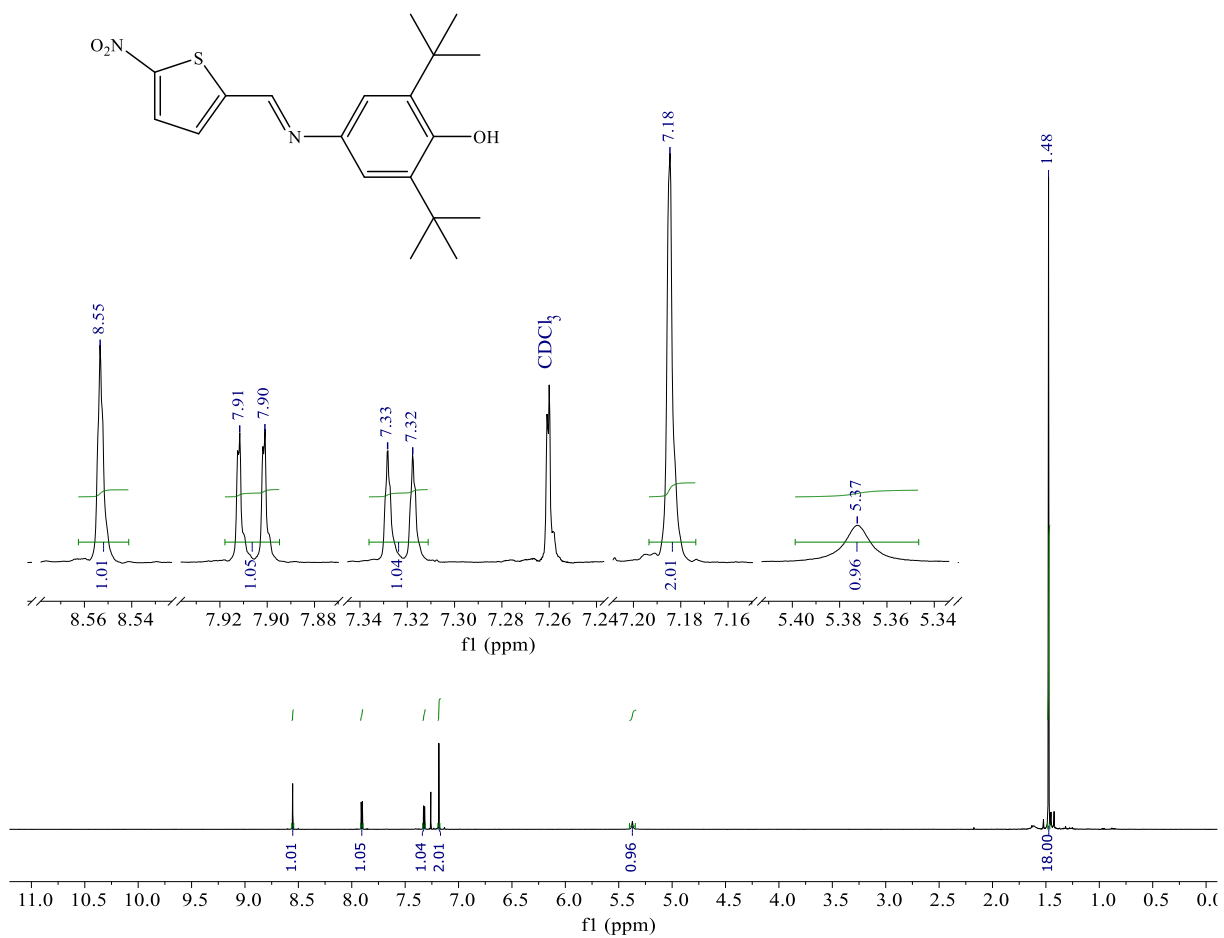


Figure S3. ¹H NMR spectrum (400 MHz, CDCl₃) of compound **5a**.

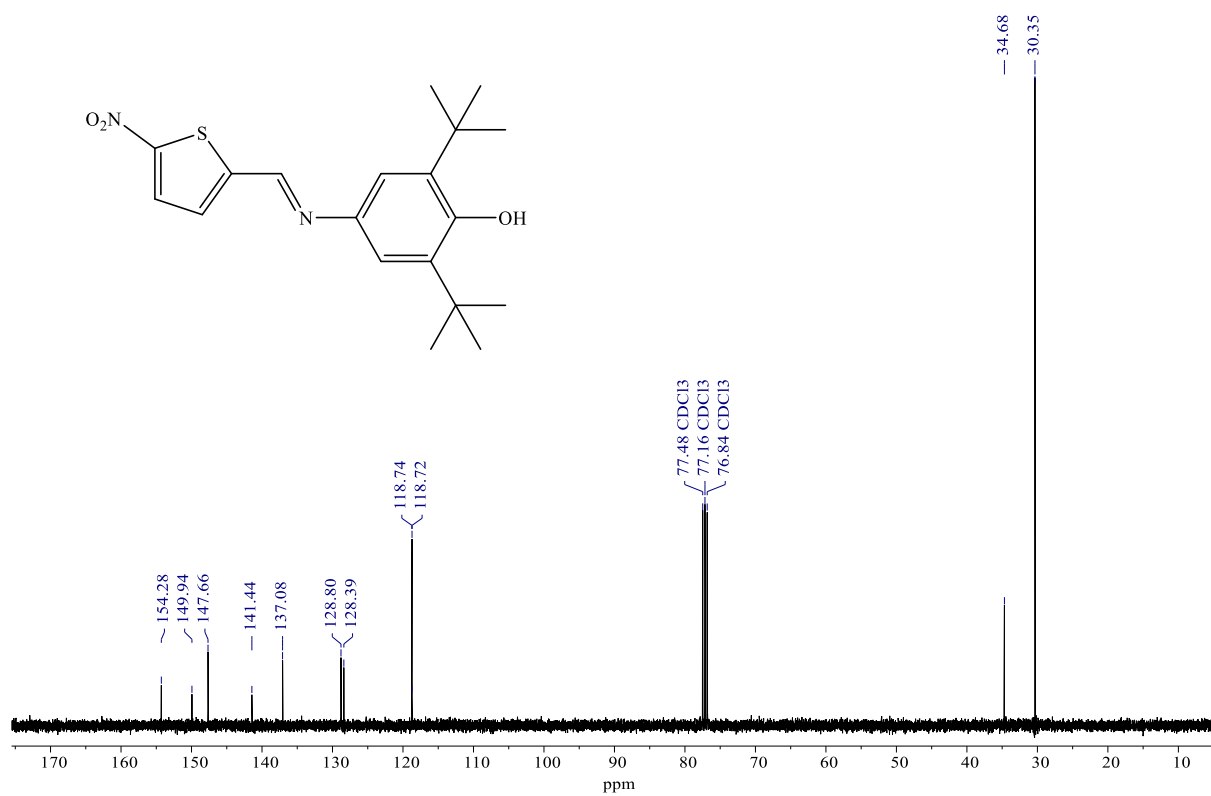


Figure S4. ^{13}C NMR spectrum (100 MHz, CDCl_3) compound of **5a**.

Display Report

Analysis Info

Analysis Name D:\Data\LabSelen 07.11\161017-A1000001.d
Method testeinicial APPI_Elis.m
Sample Name 161017-A1
Comment

Acquisition Date 11/7/2017 12:59:57 PM

Operator tofq
Instrument micrOTOF-Q 228888.10243

Acquisition Parameter

Source Type	APPI	Ion Polarity	Positive	Set Nebulizer	1.5 Bar
Focus	Not active	Set Capillary	1500 V	Set Dry Heater	200 °C
Scan Begin	50 m/z	Set End Plate Offset	-500 V	Set Dry Gas	2.0 l/min
Scan End	3000 m/z	Set Collision Cell RF	600.0 Vpp	Set Divert Valve	Source

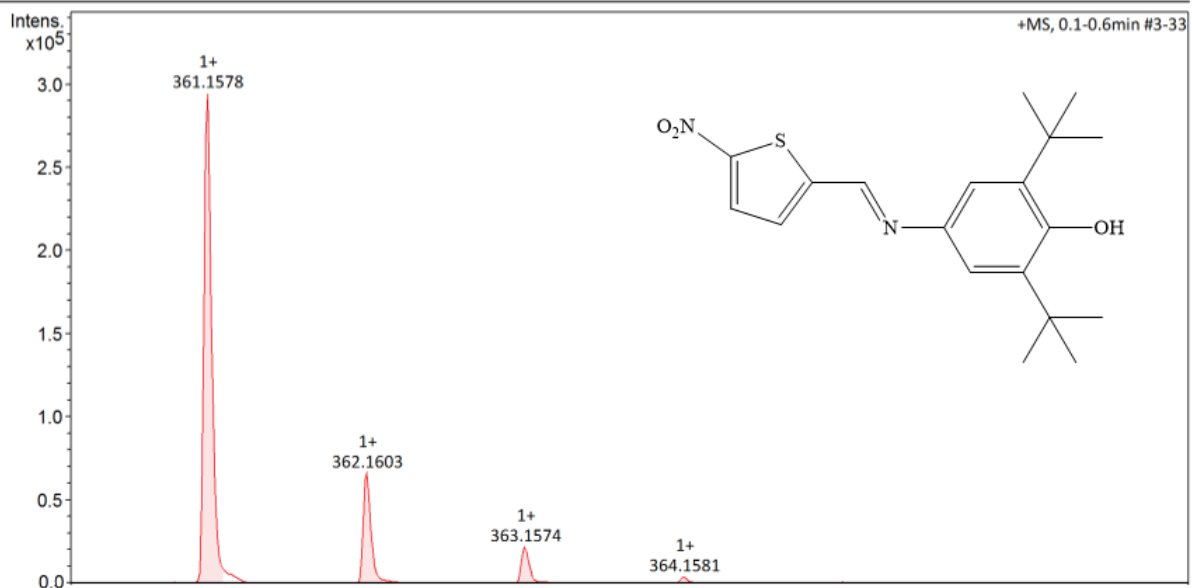


Figure S5. HRMS spectrum of compound 5a.

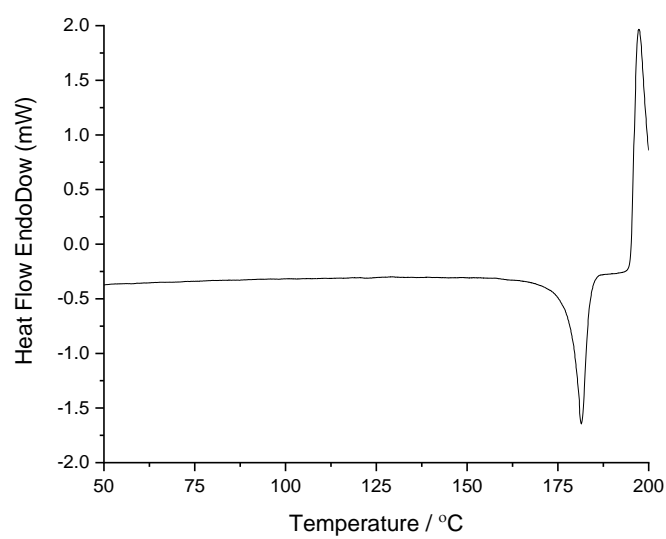


Figure S6. DSC analysis for compound **5a**. Melting temperature 181.46 °C; melting enthalpy $\Delta H_f = -82.35 \text{ J g}^{-1}$.

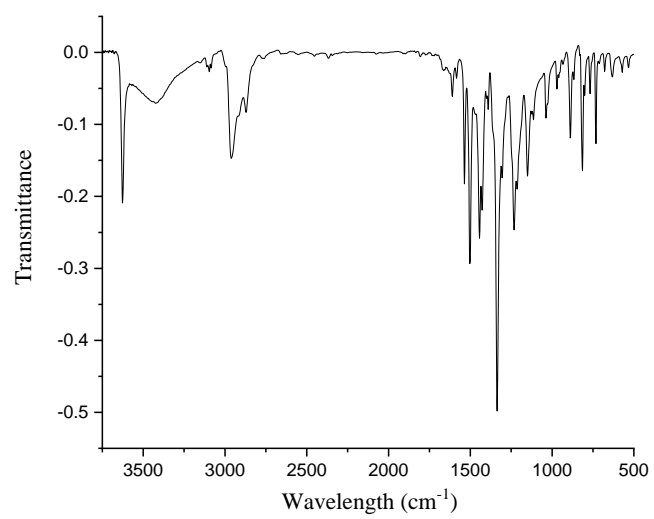


Figure S7. FTIR spectrum of **5a** (KBr pellet).

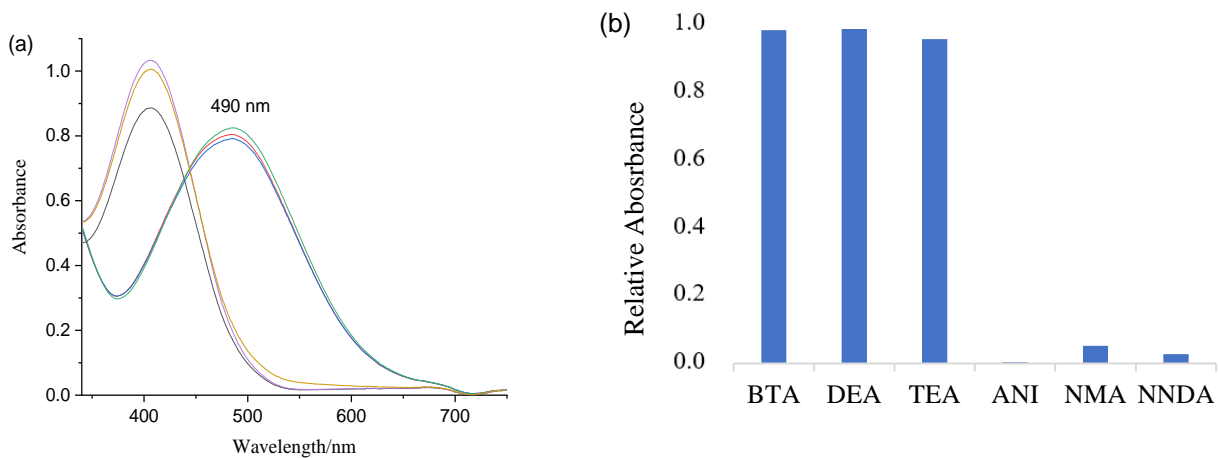


Figure S8. (a) UV-Vis spectra of the solutions of **3a** in water in the absence and after addition of BTA, DEA, TEA, ANI, NMA, and NNDA at 25.0 °C. (b) Corresponding relative absorbances. $c(\text{amine}) = 2.0 \times 10^{-4} \text{ mol L}^{-1}$.

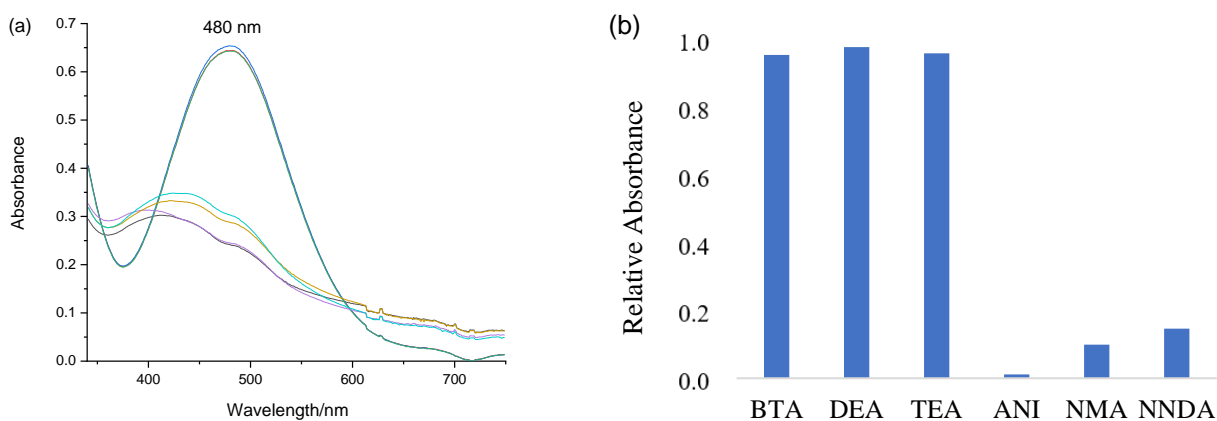


Figure S9. (a) UV-Vis spectra of the solutions of **4a** in water in the absence and after addition of BTA, DEA, TEA, ANI, NMA, and NNDA at 25.0 °C. (b) Corresponding relative absorbances. $c(\text{amine}) = 2.0 \times 10^{-4} \text{ mol L}^{-1}$.

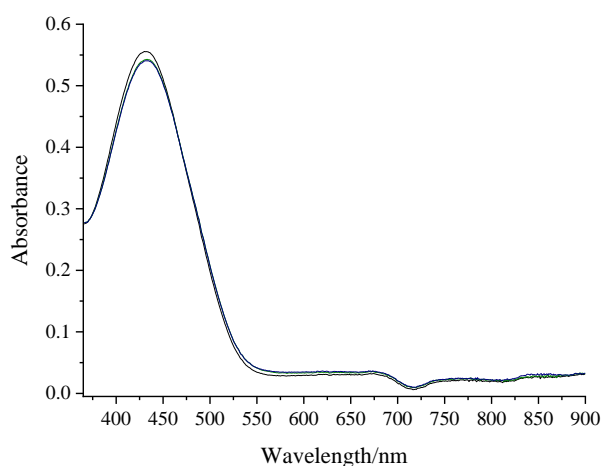


Figure S10. UV-Vis spectra of the solutions of **5a** in water in the absence and after addition of BTA, DEA, TEA, ANI, NMA, and NNDA at 25.0 °C. $c(\text{amine}) = 2.0 \times 10^{-4} \text{ mol L}^{-1}$.

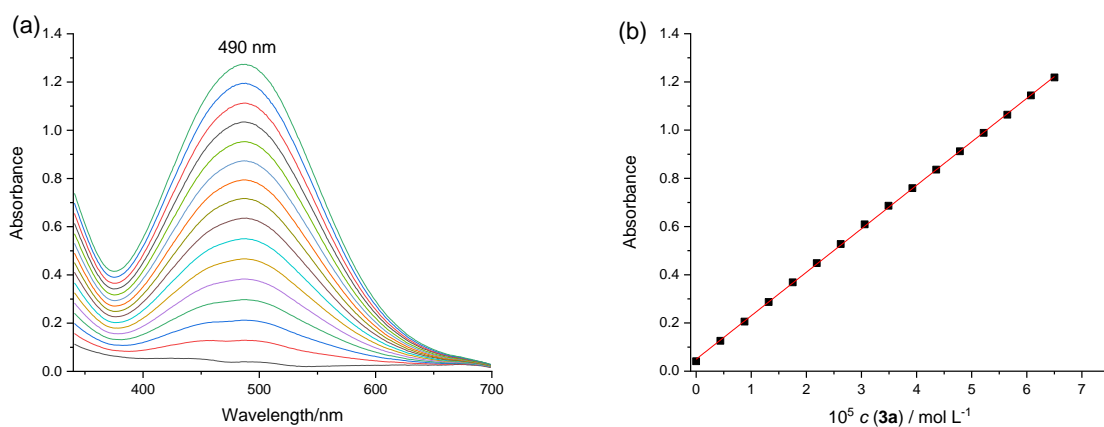


Figure S11. (a) UV-Vis spectra and (b) absorbances at 490 nm for increasing amounts of **3b** in water at 25.0 °C. Compound **3a** was deprotonated using $c(\text{BTA}) = 1.0 \times 10^{-3} \text{ mol L}^{-1}$. Data were fitted through a linear equation (—), providing $\epsilon_{\text{max}} = (1.804 \pm 0.006) \times 10^4 \text{ L mol}^{-1} \text{ cm}^{-1}$ ($r^2 = 0.999$).

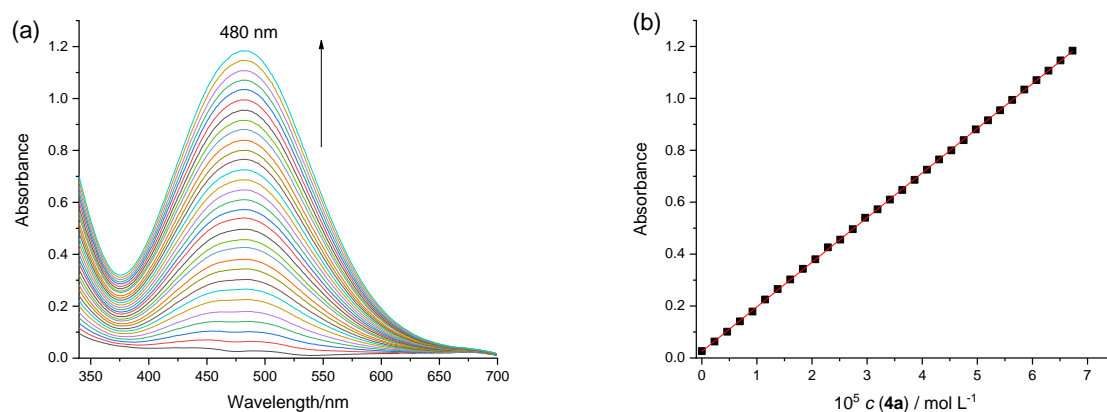


Figure S12. (a) UV-Vis spectra and (b) absorbances at 480 nm for increasing amounts of **4b** in water at 25.0 °C. Compound **4a** was deprotonated using $c(\text{BTA}) = 1.0 \times 10^{-3} \text{ mol L}^{-1}$. Data were fitted through a linear equation (—), providing $\epsilon_{\text{max}} = (1.719 \pm 0.003) \times 10^4 \text{ L mol}^{-1} \text{ cm}^{-1}$ ($r^2 = 0.999$).

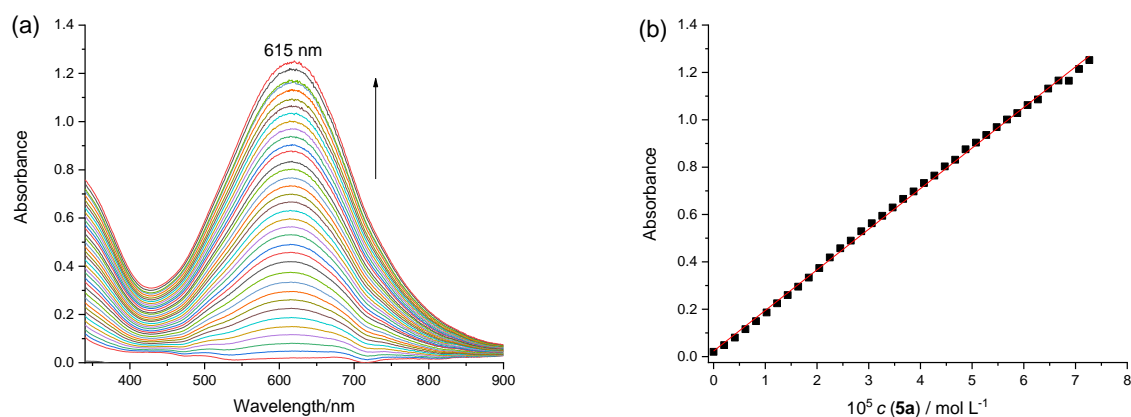


Figure S13. (a) UV-Vis spectra and (b) absorbances at 615 nm for increasing amounts of **5b** in water at 25.0 °C. Compound **5a** was deprotonated using $c(\text{NaOH}) = 1.0 \text{ mol L}^{-1}$. Data were fitted through a linear equation (—), providing $\epsilon_{\text{max}} = (1.715 \pm 0.010) \times 10^4 \text{ L mol}^{-1} \text{ cm}^{-1}$ ($r^2 = 0.999$).

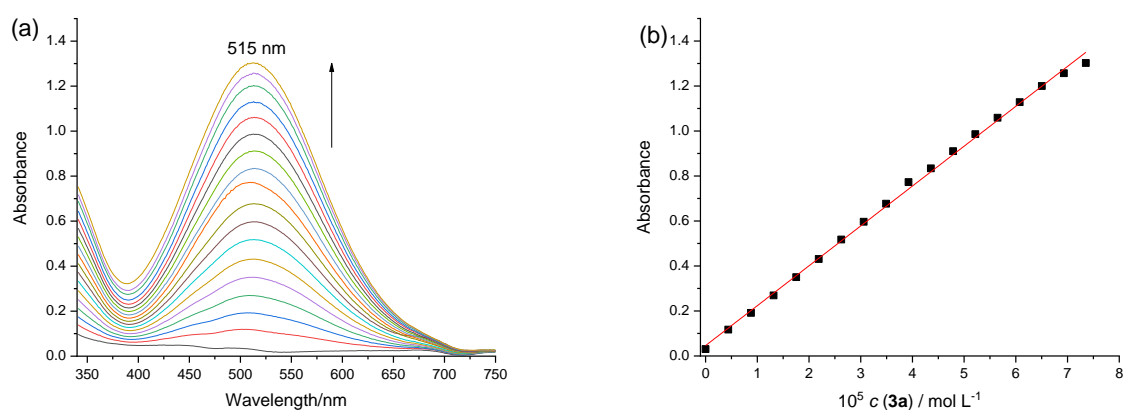


Figure S14. (a) UV-Vis spectra and (b) absorbances at 515 nm for increasing amounts of **3b** in water containing CTAB ($1.0 \times 10^{-3} \text{ mol L}^{-1}$) at 25.0 °C. Compound **3a** was deprotonated using $c(\text{BTA}) = 1.0 \times 10^{-3} \text{ mol L}^{-1}$. Data were fitted through a linear equation (—), providing $\epsilon_{\text{max}} = (1.773 \pm 0.019) \times 10^4 \text{ L mol}^{-1} \text{ cm}^{-1}$ ($r^2 = 0.998$).

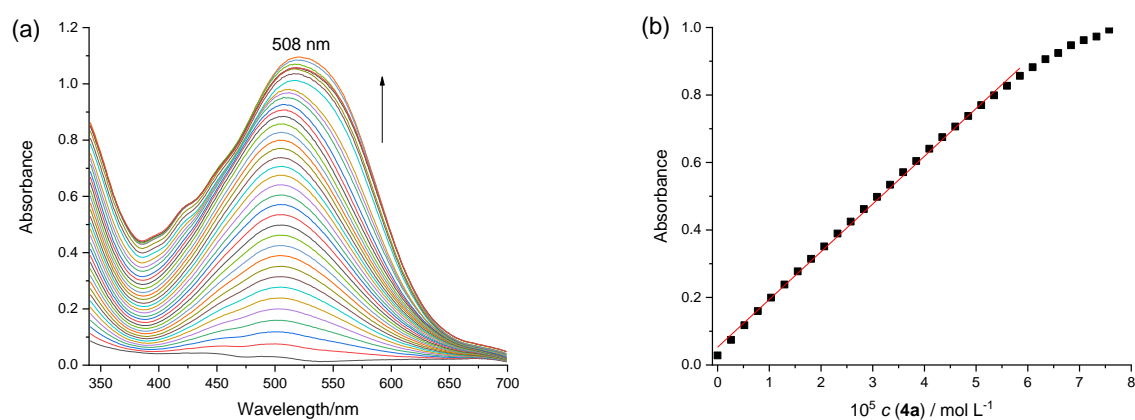


Figure S15. (a) UV-Vis spectra and (b) absorbances at 508 nm for increasing amounts of **4b** in water containing CTAB ($1.0 \times 10^{-3} \text{ mol L}^{-1}$) at 25.0 °C. Compound **4a** was deprotonated using $c(\text{BTA}) = 1.0 \times 10^{-3} \text{ mol L}^{-1}$. Data were fitted through a linear equation (—), providing $\epsilon_{\text{max}} = (1.415 \pm 0.013) \times 10^4 \text{ L mol}^{-1} \text{ cm}^{-1}$ ($r^2 = 0.998$).

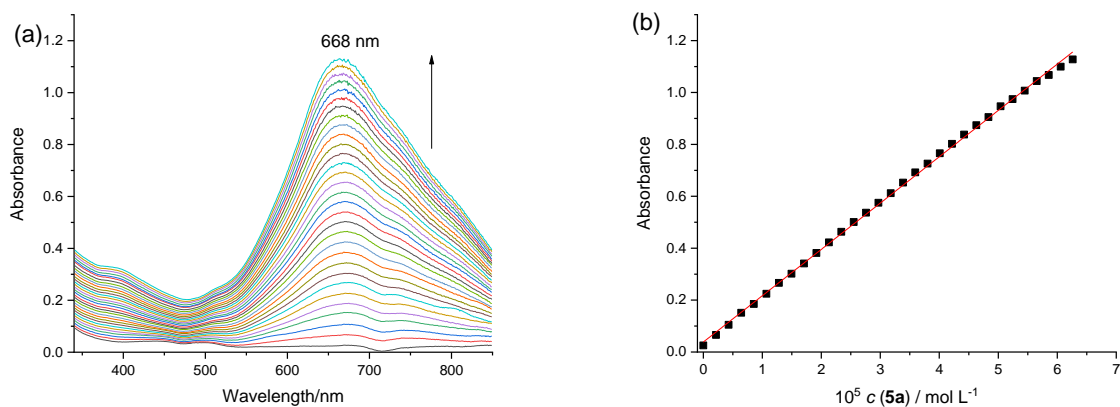


Figure S16. (a) UV-vis spectra and (b) absorbances at 668 nm for increasing amounts of **5b** in water containing CTAB ($1.0 \times 10^{-3} \text{ mol L}^{-1}$) at $25.0 \text{ }^\circ\text{C}$. Compound **5a** was deprotonated using $c(\text{BTA}) = 1.0 \times 10^{-3} \text{ mol L}^{-1}$. Data were fitted through a linear equation (—), providing $\epsilon_{\text{max}} = (1.785 \pm 0.010) \times 10^4 \text{ L mol}^{-1} \text{ cm}^{-1}$ ($r^2 = 0.999$).

Table S1. Values of $\text{p}K_{\text{a}}$ for the protonated form of the amines utilized in this paper

Protonated amine	$\text{p}K_{\text{a}}$
BTA	10.59 ^a
DEA	10.98 ^a
TEA	10.65 ^a
ANI	4.58 ^b
NMA	4.85 ^b
NNDA	5.06 ^b

^aFrom Juranić;¹ ^bfrom Gohar and Habeeb.² BTA: *n*-butylamine; DEA: diethylamine; TEA: triethylamine; ANI: aniline; NMA: *N*-methylaniline; NNDA: *N,N*-dimethylaniline.

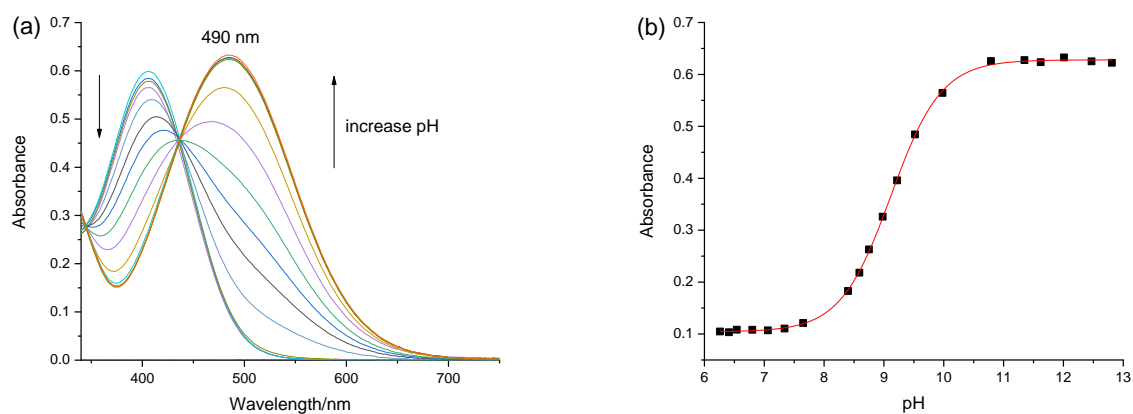


Figure S17. (a) UV-Vis spectra and (b) absorbance values for **3a** at 490 nm as a function of pH in water. Data were fitted using a sigmoidal equation, providing $pK_a = 9.11 \pm 0.01$ ($r^2 = 0.999$).

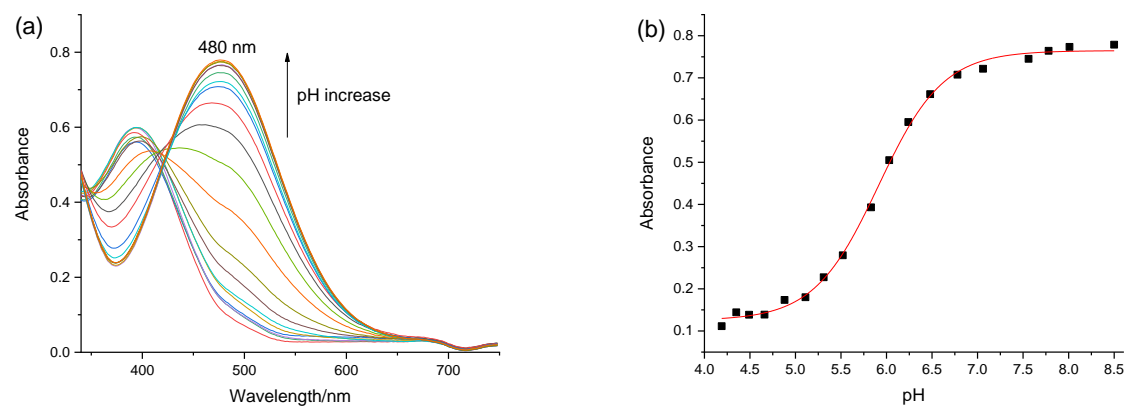


Figure S18. (a) UV-Vis spectra and (b) absorbance values for **4a** at 480 nm as a function of pH in water. Data were fitted using a sigmoidal equation, providing $pK_a = 5.91 \pm 0.01$ ($r^2 = 0.997$).

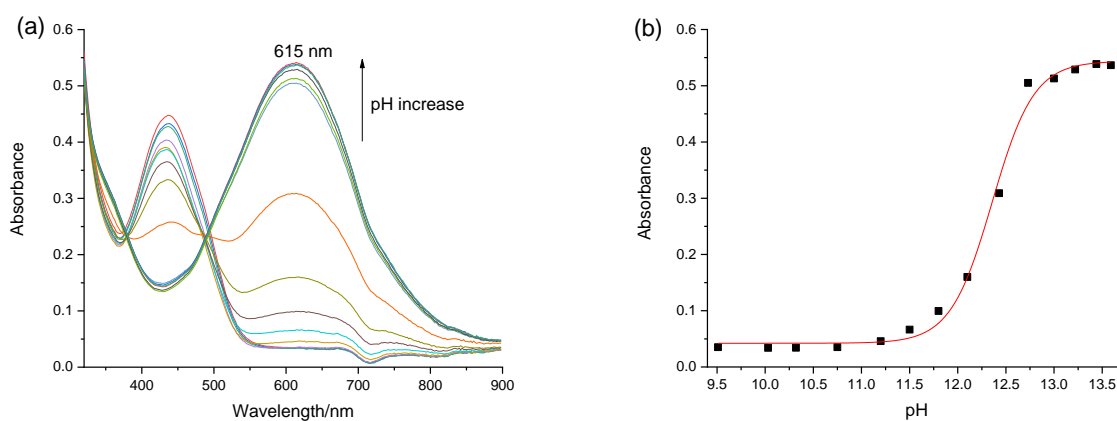


Figure S19. (a) UV-Vis spectra and (b) absorbance values for **5a** at 615 nm as a function of pH in water. Data were fitted using a sigmoidal equation, providing $pK_a = 12.35 \pm 0.02$ ($r^2 = 0.994$).

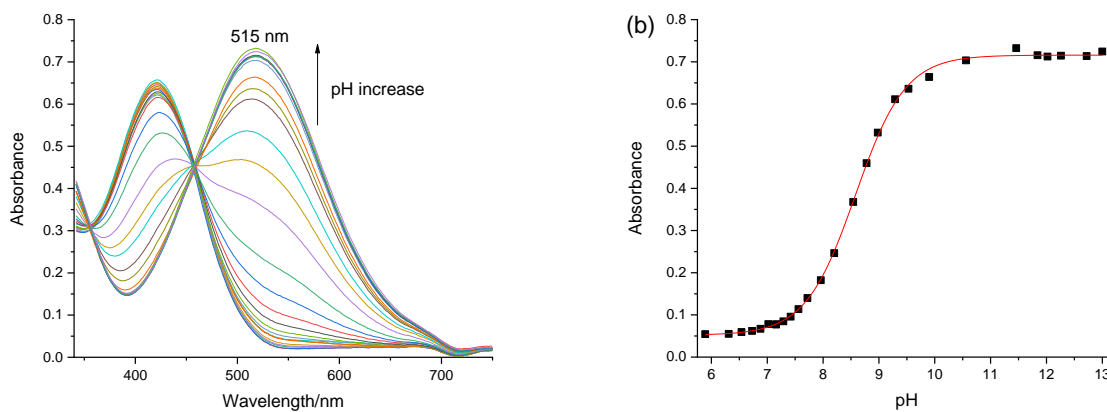


Figure S20. (a) UV-Vis spectra and (b) absorbance values for **3a** at 515 nm as a function of pH in water containing CTAB ($1.0 \times 10^{-3} \text{ mol L}^{-1}$). Data were fitted using a sigmoidal equation, providing $pK_a = 8.57 \pm 0.01$ ($r^2 = 0.999$).

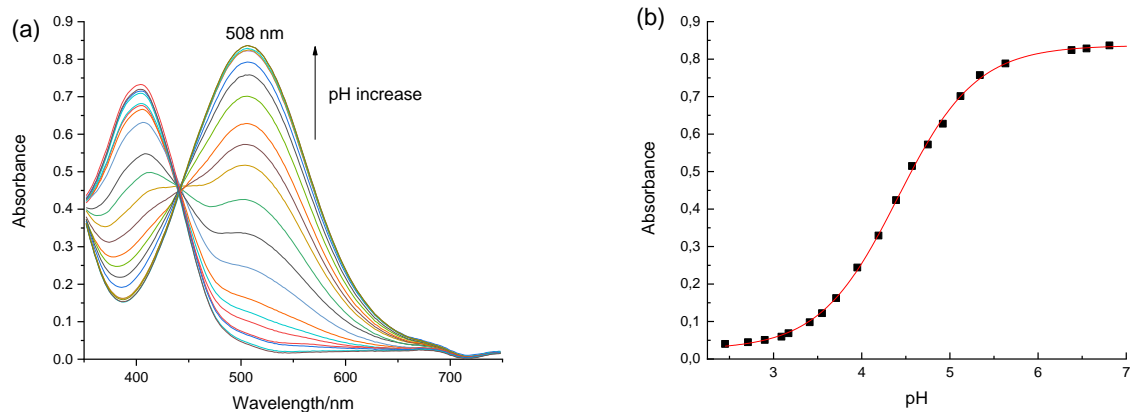


Figure S21. (a) UV-Vis spectra and (b) absorbance values for **4a** at 508 nm as a function of pH in water containing CTAB ($1.0 \times 10^{-3} \text{ mol L}^{-1}$). Data were fitted using a sigmoidal equation, providing $\text{p}K_{\text{a}} = 4.40 \pm 0.01$ ($r^2 = 0.999$).

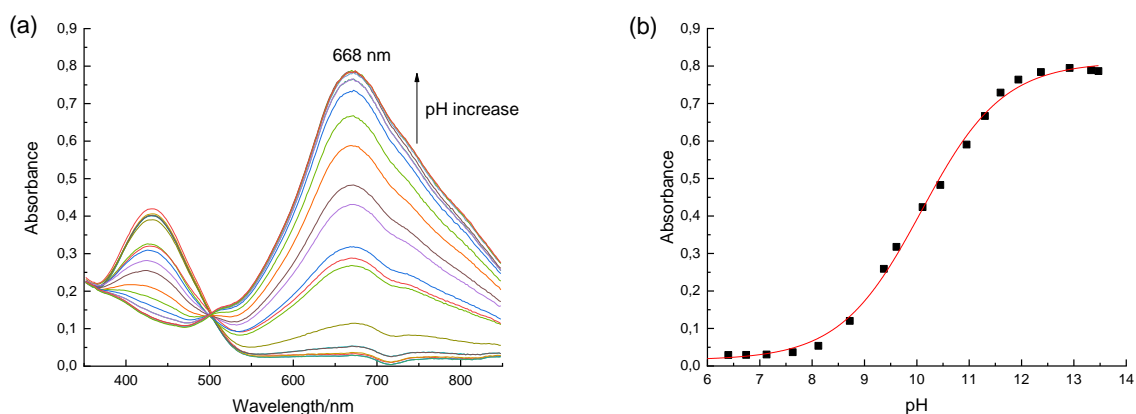


Figure S22. (a) UV-Vis spectra and (b) absorbance values for **5a** at 668 nm as a function of pH in water containing CTAB ($1.0 \times 10^{-3} \text{ mol L}^{-1}$). Data were fitted using a sigmoidal equation, providing $\text{p}K_{\text{a}} = 10.08 \pm 0.02$ ($r^2 = 0.999$).

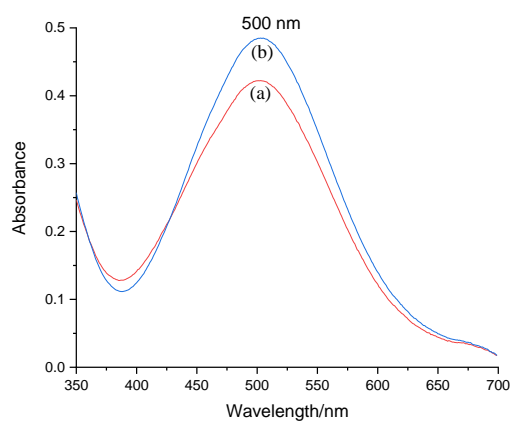


Figure S23. UV-Vis spectra of the solutions of **4a** in water in the absence (a) and after addition of BTA (b) at 25.0 °C. $c(\text{amine}) = 2.0 \times 10^{-4} \text{ mol L}^{-1}$.

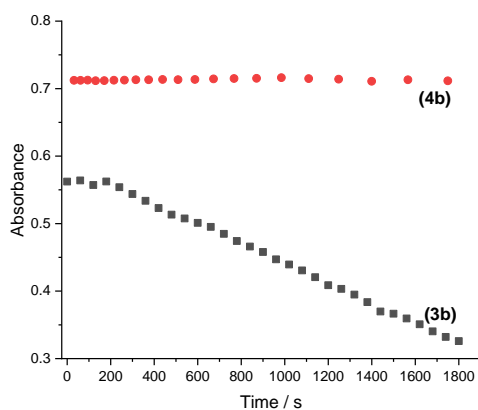


Figure S24. Stability assays of **3b** and **4b** ($4.0 \times 10^{-5} \text{ mol L}^{-1}$) in aqueous medium at 25.0 °C. The absorbance values were collected at λ_{max} at 486 and 480 nm for **3a** and **4a**, respectively (pH = 7.0 and $c(\text{BTA}) = 2.0 \times 10^{-3} \text{ mol L}^{-1}$).

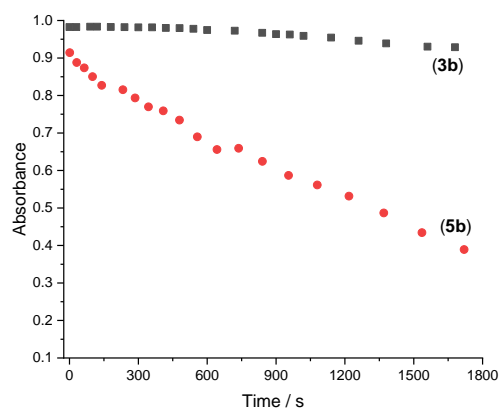


Figure S25. Stability assays of **3a** ($5.0 \times 10^{-5} \text{ mol L}^{-1}$) and **5a** ($4.8 \times 10^{-5} \text{ mol L}^{-1}$) in aqueous medium containing CTAB ($1.0 \times 10^{-3} \text{ mol L}^{-1}$) at $25.0 \text{ }^\circ\text{C}$. The absorbance values were collected at λ_{max} at 515 and 668 nm for **3a** and **5a**, respectively ($\text{pH} = 7.0$ and $c(\text{BTA}) = 2.0 \times 10^{-3} \text{ mol L}^{-1}$).

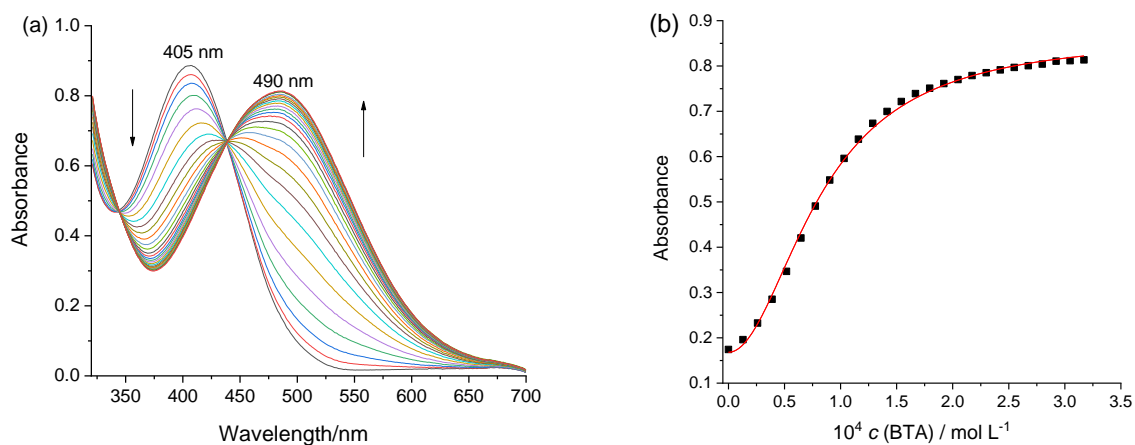


Figure S26. (a) UV-Vis spectra for titration of compound **3a** ($4.0 \times 10^{-5} \text{ mol L}^{-1}$) with BTA in aqueous medium at $25.0 \text{ }^\circ\text{C}$. (b) Corresponding titration curve, with absorbances collected at 490 nm. $K_{12} = (1.463 \pm 0.048) \times 10^8 \text{ L}^2 \text{ mol}^{-2}$ ($r^2 = 0.998$; $\text{SD} = 5.02 \times 10^{-3}$).

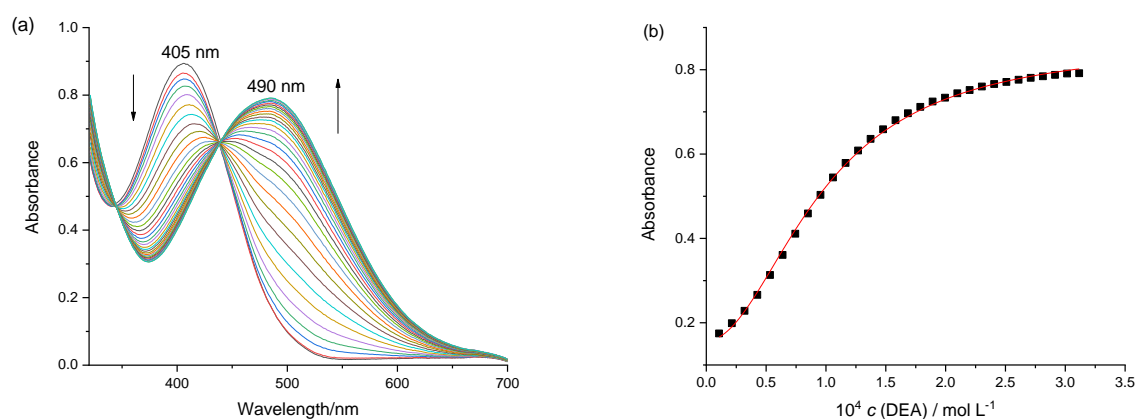


Figure S27. (a) UV-Vis spectra for titration of compound **3a** ($4.0 \times 10^{-5} \text{ mol L}^{-1}$) with DEA in aqueous medium at $25.0 \text{ }^\circ\text{C}$. (b) Corresponding titration curve, with absorbances collected at 490 nm . $K_{12} = (1.070 \pm 0.028) \times 10^8 \text{ L}^2 \text{ mol}^{-2}$ ($r^2 = 0.999$; $\text{SD} = 4.05 \times 10^{-3}$).

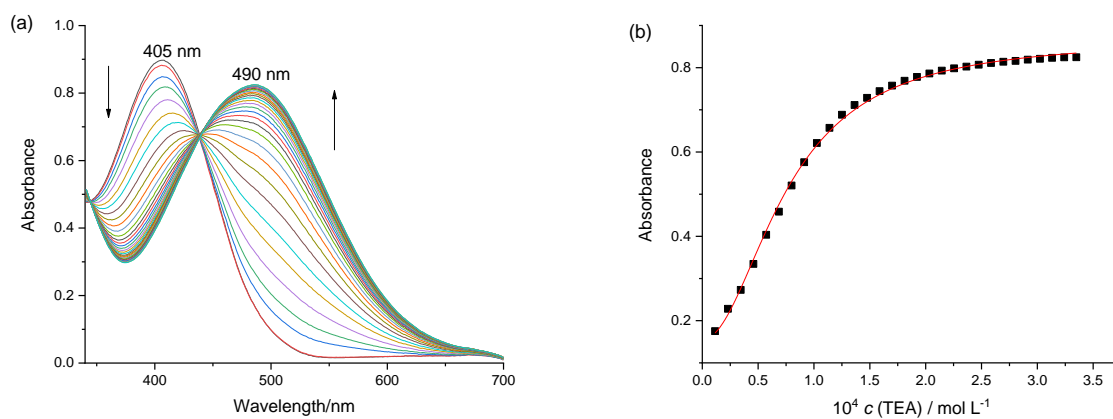


Figure S28. (a) UV-Vis spectra for titration of compound **3a** ($4.0 \times 10^{-5} \text{ mol L}^{-1}$) with TEA in aqueous medium at $25.0 \text{ }^\circ\text{C}$. (b) Corresponding titration curve, with absorbances collected at 486 nm . $K_{12} = (1.729 \pm 0.055) \times 10^8 \text{ L}^2 \text{ mol}^{-2}$ ($r^2 = 0.998$; $\text{SD} = 5.92 \times 10^{-3}$).

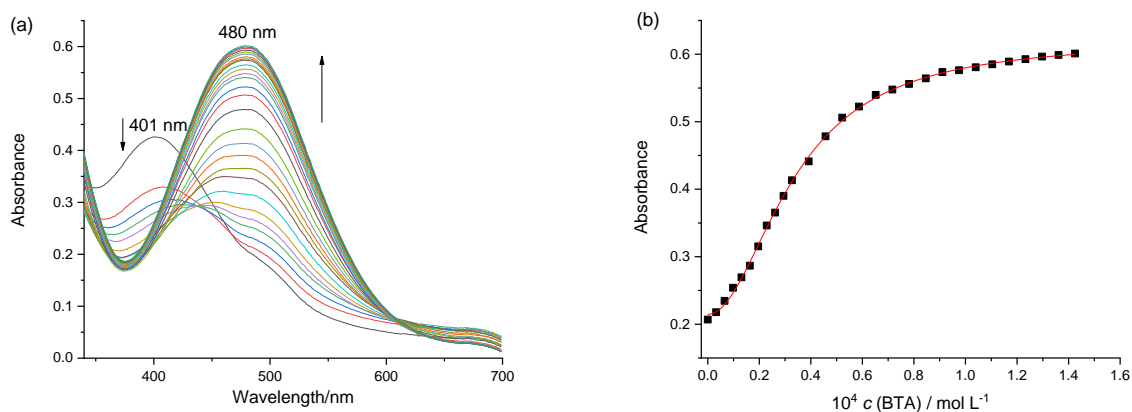


Figure S29. (a) UV-Vis spectra for titration of compound **4a** ($4.0 \times 10^{-5} \text{ mol L}^{-1}$) with BTA in aqueous medium at $25.0 \text{ }^\circ\text{C}$. (b) Corresponding titration curve, with absorbances collected at 480 nm . $K_{12} = (8.797 \pm 0.191) \times 10^8 \text{ L}^2 \text{ mol}^{-2}$ ($r^2 = 0.999$; $\text{SD} = 1.78 \times 10^{-3}$).

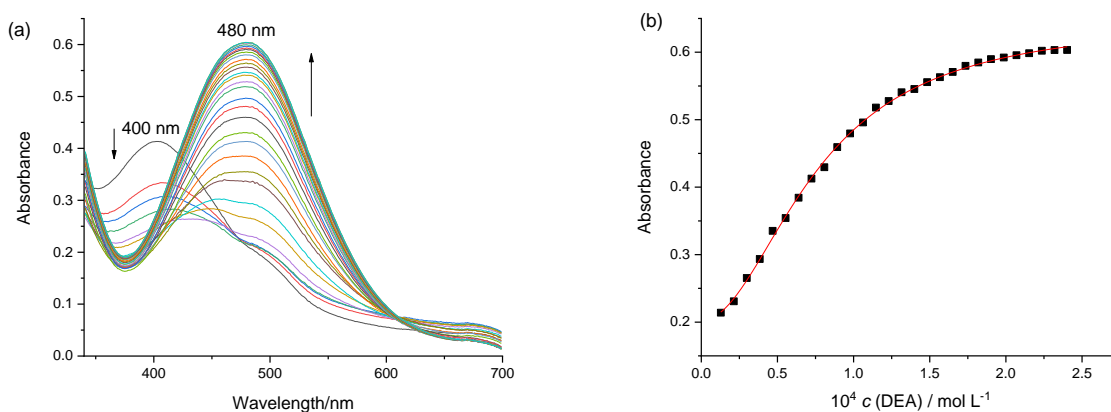


Figure S30. (a) UV-Vis spectra for titration of compound **4a** ($4.0 \times 10^{-5} \text{ mol L}^{-1}$) with DEA in aqueous medium at $25.0 \text{ }^\circ\text{C}$. (b) Corresponding titration curve, with absorbances collected at 480 nm . $K_{12} = (1.721 \pm 0.044) \times 10^8 \text{ L}^2 \text{ mol}^{-2}$ ($r^2 = 0.999$; $\text{SD} = 2.62 \times 10^{-3}$).

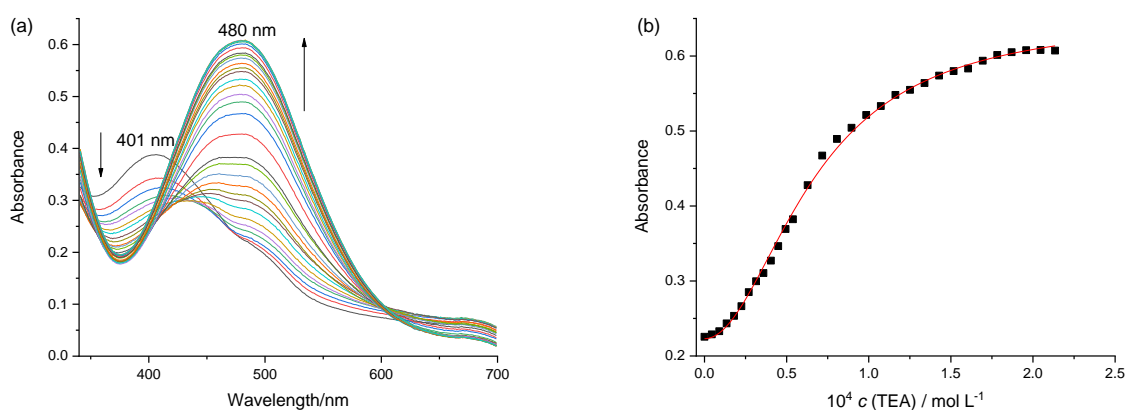


Figure S31. (a) UV-Vis spectra for titration of compound **4a** ($4.0 \times 10^{-5} \text{ mol L}^{-1}$) with TEA in aqueous medium at $25.0 \text{ }^\circ\text{C}$. (b) Corresponding titration curve, with absorbances collected at 480 nm . $K_{12} = (2.237 \pm 0.080) \times 10^8 \text{ L}^2 \text{ mol}^{-2}$ ($r^2 = 0.998$; $\text{SD} = 2.61 \times 10^{-3}$).

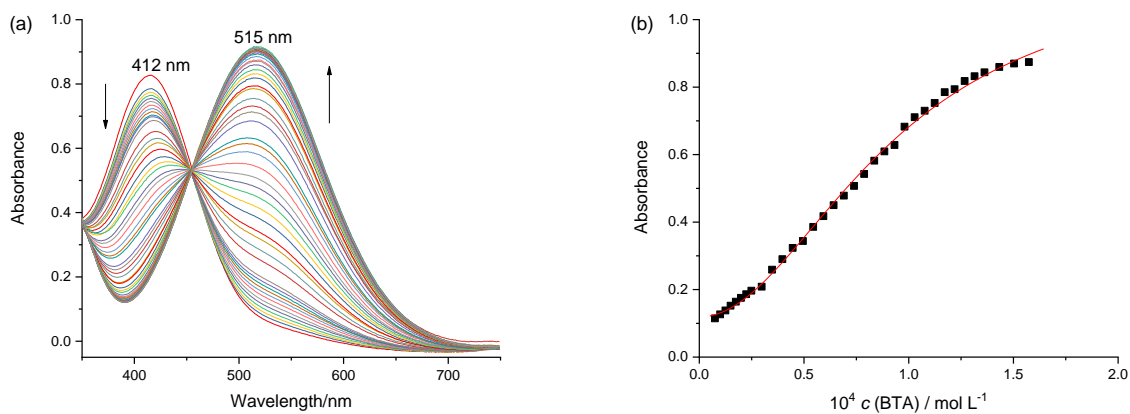


Figure S32. (a) UV-Vis spectra for titration of compound **3a** ($4.0 \times 10^{-5} \text{ mol L}^{-1}$) with BTA in aqueous medium containing CTAB ($1.0 \times 10^{-3} \text{ mol L}^{-1}$) at $25.0 \text{ }^\circ\text{C}$. (b) Corresponding titration curve, with absorbances collected at 515 nm . $K_{12} = (1.162 \pm 0.050) \times 10^8 \text{ L}^2 \text{ mol}^{-2}$ ($r^2 = 0.997$; $\text{S.D.} = 4.63 \times 10^{-3}$).

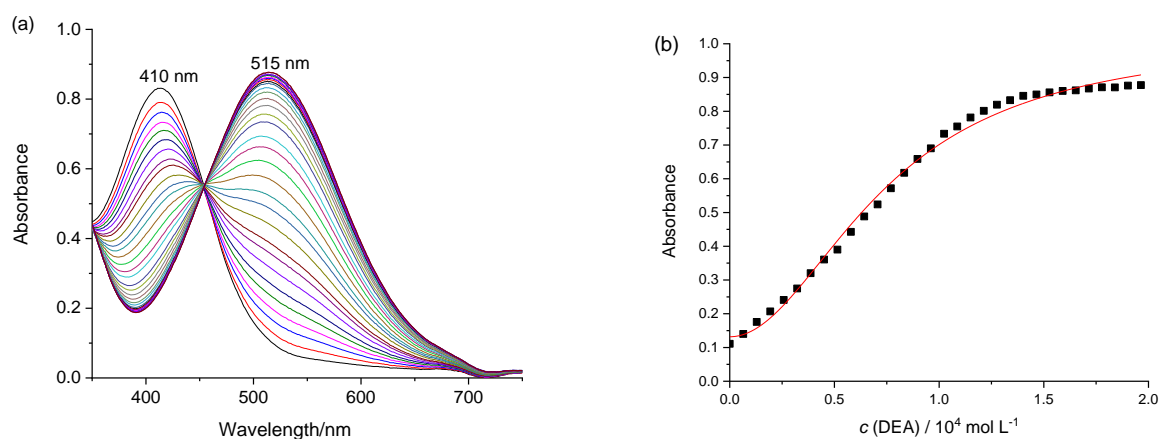


Figure S33. (a) UV-Vis spectra for titration of compound **3a** ($4.0 \times 10^{-5} \text{ mol L}^{-1}$) with DEA in aqueous medium containing CTAB ($1.0 \times 10^{-3} \text{ mol L}^{-1}$) at $25.0 \text{ }^\circ\text{C}$. (b) Corresponding titration curve, with absorbances collected at 515 nm. $K_{12} = (1.173 \pm 0.049) \times 10^8 \text{ L}^2 \text{ mol}^{-2}$ ($r^2 = 0.995$; $\text{SD} = 3.29 \times 10^{-3}$).

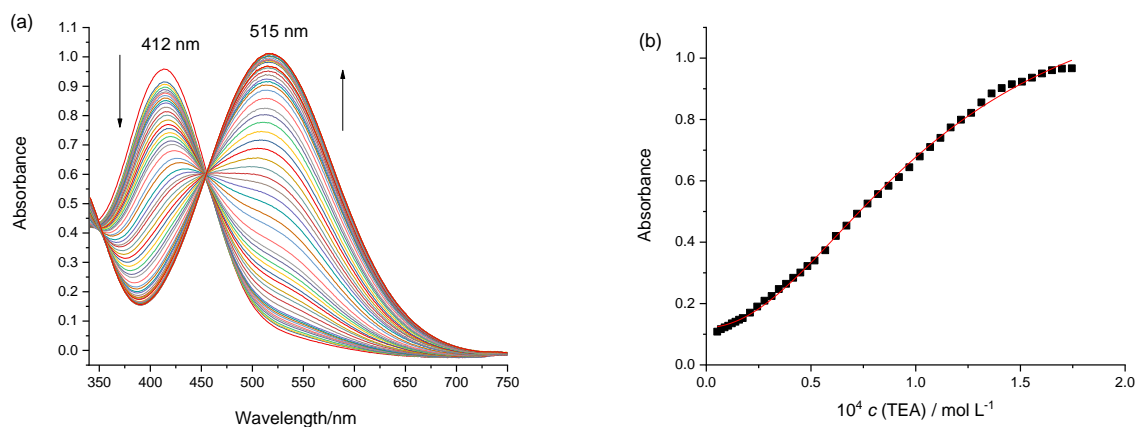


Figure S34. (a) UV-Vis spectra for titration of compound **3a** ($4.0 \times 10^{-5} \text{ mol L}^{-1}$) with TEA in aqueous medium containing CTAB ($1.0 \times 10^{-3} \text{ mol L}^{-1}$) at $25.0 \text{ }^\circ\text{C}$. (b) Corresponding titration curve, with absorbances collected at 515 nm. $K_{12} = (8.511 \pm 0.262) \times 10^7 \text{ L}^2 \text{ mol}^{-2}$ ($r^2 = 0.995$; $\text{SD} = 3.29 \times 10^{-3}$).

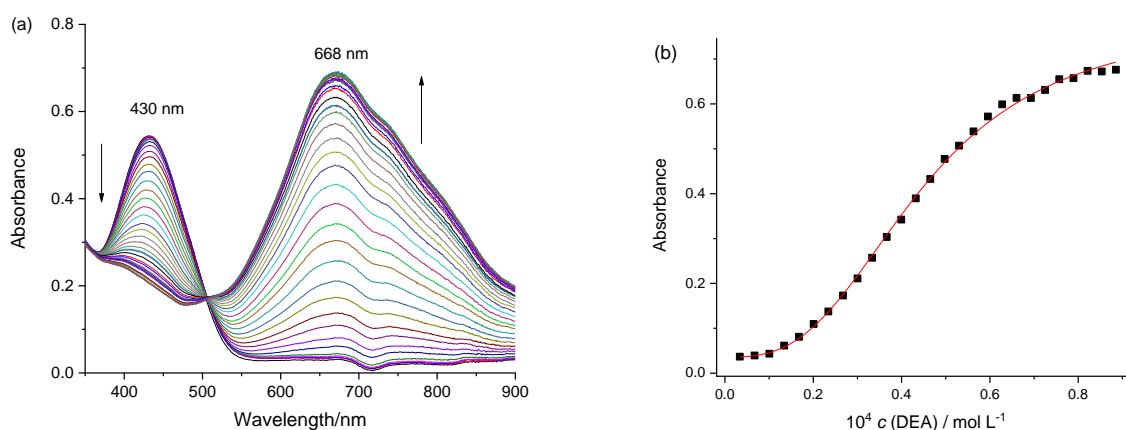


Figure S35. (a) UV-Vis spectra for titration of compound **5a** ($4.0 \times 10^{-5} \text{ mol L}^{-1}$) with DEA in aqueous medium containing CTAB ($1.0 \times 10^{-3} \text{ mol L}^{-1}$) at 25.0 °C. (b) Corresponding titration curve, with absorbances collected at 670 nm. $K_{12} = (1.240 \pm 0.279) \times 10^8 \text{ L}^2 \text{ mol}^{-2}$ and $K_{13} = (7.160 \pm 0.182) \times 10^4 \text{ L}^3 \text{ mol}^{-3}$ ($r^2 = 0.997$; $\text{SD} = 6.17 \times 10^{-3}$).

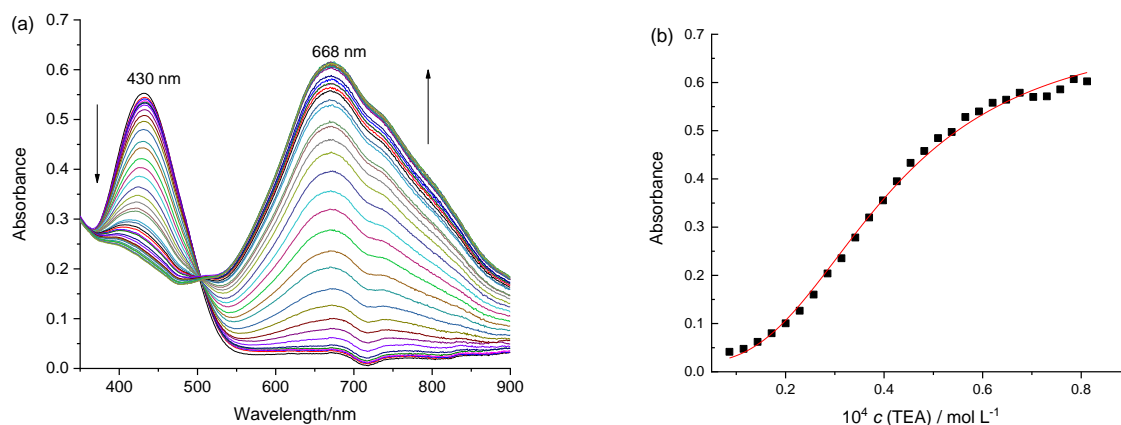


Figure S36. (a) UV-Vis spectra for titration of compound **5a** ($4.0 \times 10^{-5} \text{ mol L}^{-1}$) with TEA in aqueous medium containing CTAB ($1.0 \times 10^{-3} \text{ mol L}^{-1}$) at 25.0 °C. (b) Corresponding titration curve, with absorbances collected at 668 nm. $K_{12} = (1.844 \pm 0.325) \times 10^8 \text{ L}^2 \text{ mol}^{-2}$ and $K_{13} = (7.780 \pm 1.099) \times 10^4 \text{ L}^3 \text{ mol}^{-3}$ ($r^2 = 0.998$; $\text{SD} = 5.44 \times 10^{-3}$).

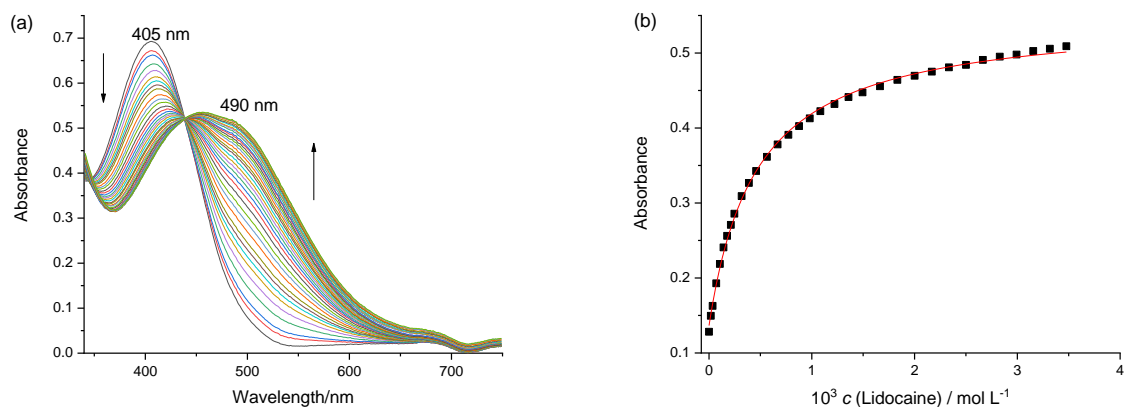


Figure S37. (a) UV-Vis spectra for titration of compound **3a** ($5.0 \times 10^{-5} \text{ mol L}^{-1}$) with lidocaine in aqueous medium at $25.0 \text{ }^\circ\text{C}$. (b) Corresponding titration curve, with absorbances collected at 490 nm . $K_{11} = (2.164 \pm 0.006 \times 10^3 \text{ L mol}^{-1})$ ($r^2 = 0.998$; $\text{SD} = 2.53 \times 10^{-3}$).

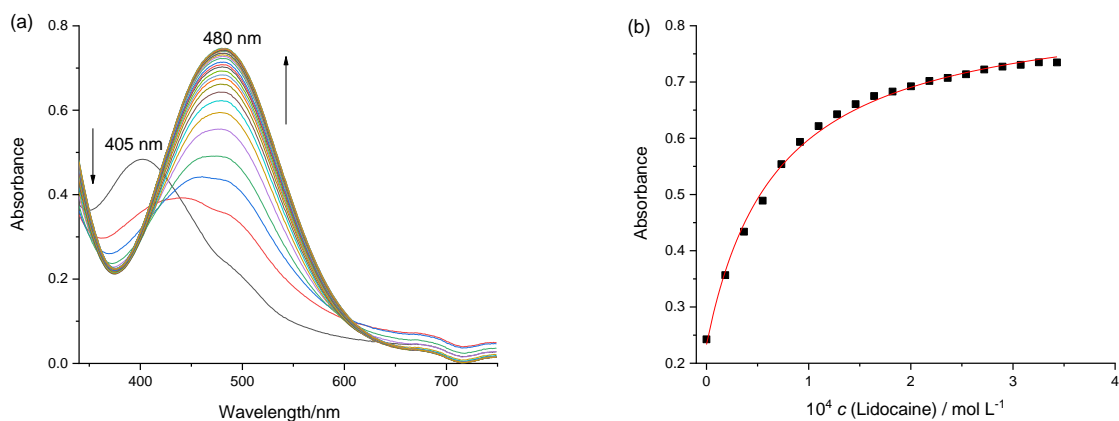


Figure S38. (a) UV-Vis spectra for titration of compound **4a** ($5.0 \times 10^{-5} \text{ mol L}^{-1}$) with lidocaine in aqueous medium at $25.0 \text{ }^\circ\text{C}$. (b) Corresponding titration curve, with absorbances collected at 480 nm . $K_{11} = (1.493 \pm 0.088) \times 10^4 \text{ L mol}^{-1}$ ($r^2 = 0.995$; $\text{SD} = 7.91 \times 10^{-3}$).

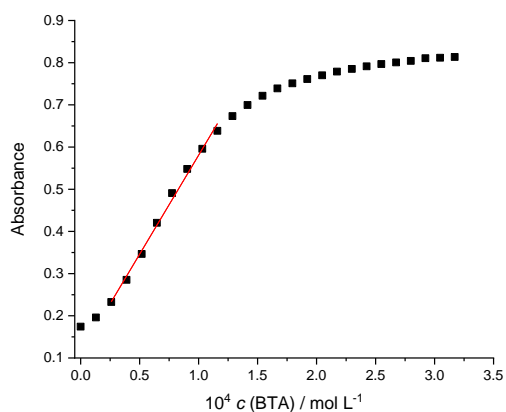


Figure S39. Curve for the titration of **3a** with BTA in aqueous medium, utilized to estimate values of LOD and LOQ. Fitting of experimental data (—), LOD = 2.36×10^{-6} mol L⁻¹, and LOQ = 7.88×10^{-6} mol L⁻¹ ($r^2 = 0.993$; SD = 1.11×10^{-2}).

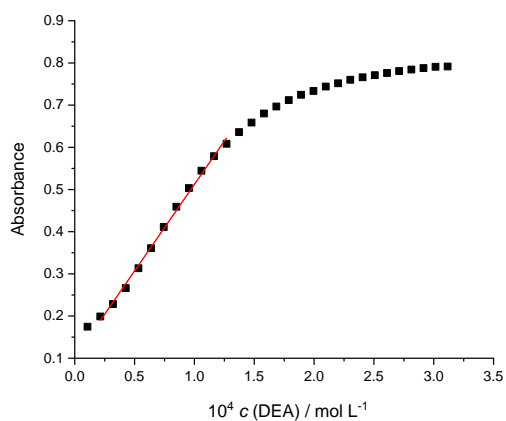


Figure S40. Curve for the titration of **3a** with DEA in aqueous medium, utilized to estimate values of LOD and LOQ. Fitting of experimental data (—), LOD = 1.61×10^{-6} mol L⁻¹, and LOQ = 5.36×10^{-6} mol L⁻¹ ($r^2 = 0.996$; SD = 6.61×10^{-3}).

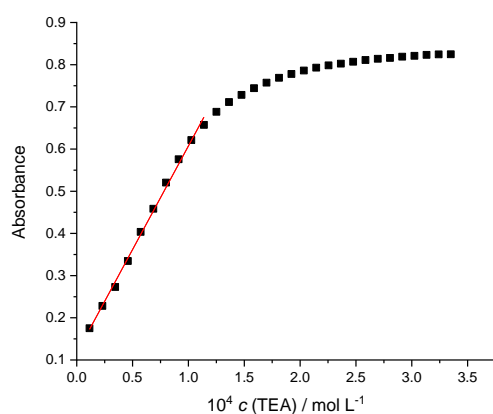


Figure S41. Curve for the titration of **3a** with TEA in aqueous medium, utilized to estimate values of LOD and LOQ. Fitting of experimental data (—), LOD = 1.45×10^{-6} mol L⁻¹, and LOQ = 4.18×10^{-6} mol L⁻¹ ($r^2 = 0.996$; SD = 7.09×10^{-3}).

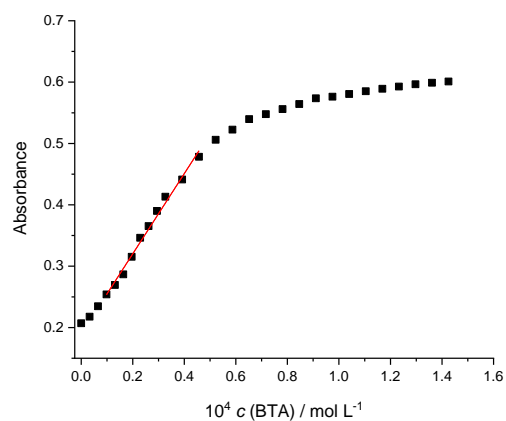


Figure S42. Curve for the titration of **4a** with BTA in aqueous medium, utilized to estimate values of LOD and LOQ. Fitting of experimental data (—), LOD = 9.71×10^{-7} mol L⁻¹, and LOQ = 3.23×10^{-6} mol L⁻¹ ($r^2 = 0.989$; SD = 3.35×10^{-3}).

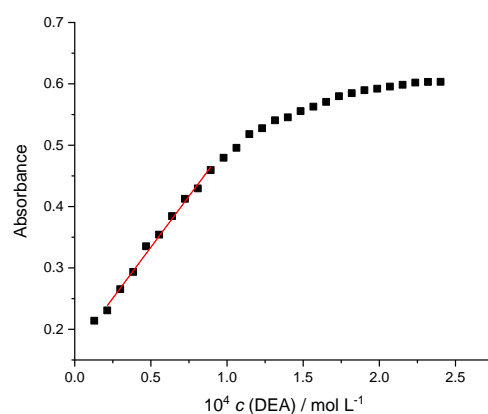


Figure S43. Curve for the titration of **4a** with DEA in aqueous medium, utilized to estimate values of LOD and LOQ. Fitting of experimental data (—), LOD = $1.84 \times 10^{-6} \text{ mol L}^{-1}$, and LOQ = $6.54 \times 10^{-6} \text{ mol L}^{-1}$ ($r^2 = 0.989$; SD = 6.14×10^{-3}).

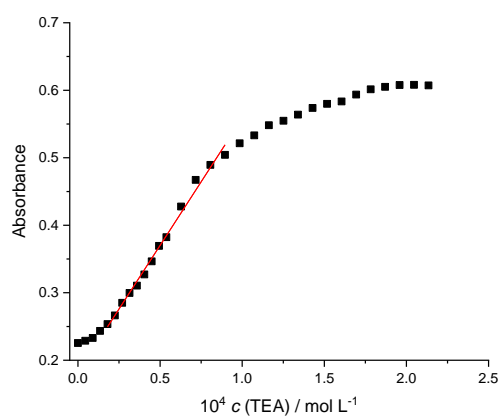


Figure S44. Curve for the titration of **4a** with TEA in aqueous medium, utilized to estimate values of LOD and LOQ. Fitting of experimental data (—), LOD = $1.42 \times 10^{-6} \text{ mol L}^{-1}$, and LOQ = $4.75 \times 10^{-6} \text{ mol L}^{-1}$ ($r^2 = 0.991$; SD = 5.38×10^{-3}).

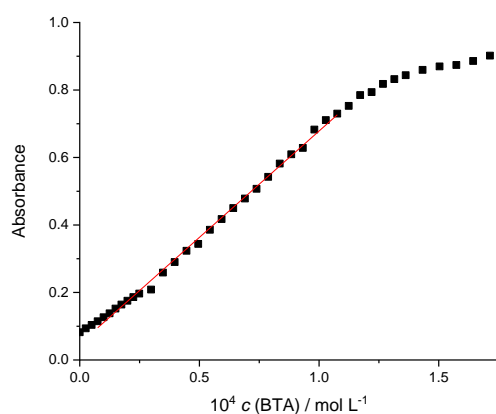


Figure S45. Curve for the titration of **3a** with BTA in water containing CTAB ($1.0 \times 10^{-3} \text{ mol L}^{-1}$), utilized to estimate values of LOD and LOQ. Fitting of experimental data (—), LOD = $6.89 \times 10^{-7} \text{ mol L}^{-1}$, and LOQ = $2.29 \times 10^{-6} \text{ mol L}^{-1}$ ($r^2 = 0.997$; SD = 4.43×10^{-3}).

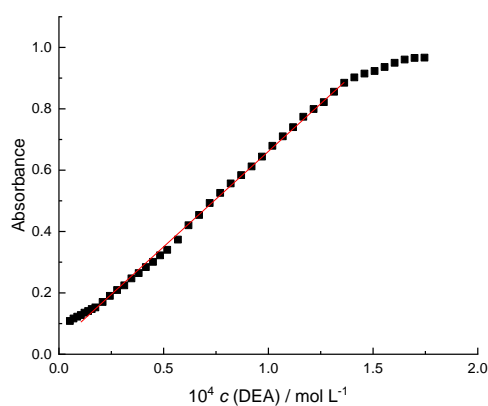


Figure S46. Curve for the titration of **3a** with DEA in water containing CTAB ($1.0 \times 10^{-3} \text{ mol L}^{-1}$), utilized to estimate values of LOD and LOQ. Fitting of experimental data (—), LOD = $5.29 \times 10^{-7} \text{ mol L}^{-1}$, and LOQ = $1.76 \times 10^{-6} \text{ mol L}^{-1}$ ($r^2 = 0.998$; SD = 6.72×10^{-3}).

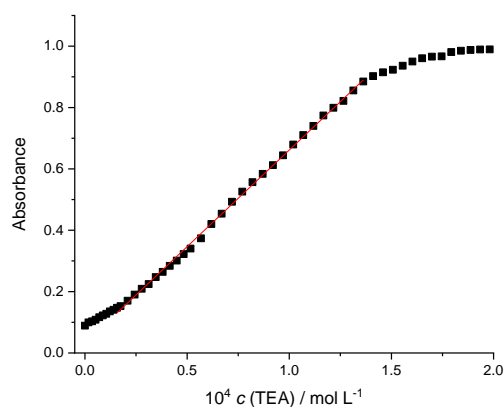


Figure S47. Curve for the titration of **3a** with TEA in water containing CTAB ($1.0 \times 10^{-3} \text{ mol L}^{-1}$), utilized to estimate values of LOD and LOQ. Fitting of experimental data (—), LOD = $6.27 \times 10^{-7} \text{ mol L}^{-1}$, and LOQ = $2.09 \times 10^{-6} \text{ mol L}^{-1}$ ($r^2 = 0.998$; SD = 3.98×10^{-3}).

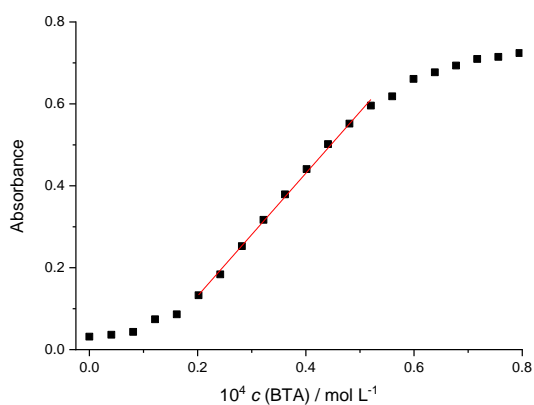


Figure S48. Curve for the titration of **5a** with BTA in water containing CTAB ($1.0 \times 10^{-3} \text{ mol L}^{-1}$), utilized to estimate values of LOD and LOQ. Fitting of experimental data (—), LOD = $7.00 \times 10^{-7} \text{ mol L}^{-1}$, and LOQ = $2.33 \times 10^{-6} \text{ mol L}^{-1}$ ($r^2 = 0.997$; SD = 1.05×10^{-2}).

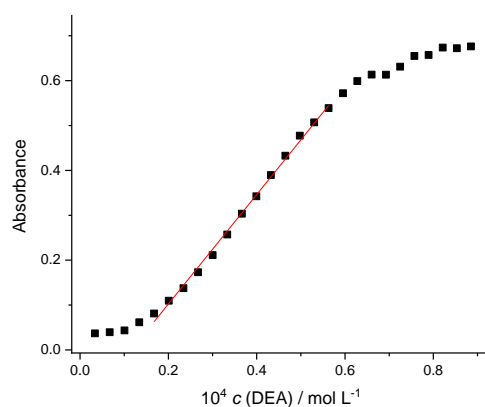


Figure S49. Curve for the titration of **5a** with DEA in water containing CTAB ($1.0 \times 10^{-3} \text{ mol L}^{-1}$), utilized to estimate values of LOD and LOQ. Fitting of experimental data (—), LOD = $6.99 \times 10^{-7} \text{ mol L}^{-1}$, and LOQ = $2.33 \times 10^{-6} \text{ mol L}^{-1}$ ($r^2 = 0.996$; SD = 8.53×10^{-3}).

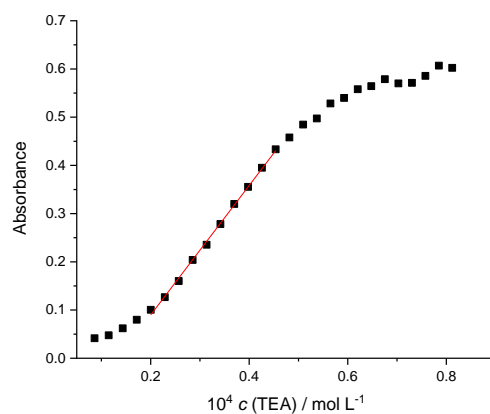


Figure S50. Curve for the titration of **5a** with TEA in water containing CTAB ($1.0 \times 10^{-3} \text{ mol L}^{-1}$), utilized to estimate values of LOD and LOQ. Fitting of experimental data (—), LOD = $5.08 \times 10^{-7} \text{ mol L}^{-1}$, and LOQ = $1.69 \times 10^{-6} \text{ mol L}^{-1}$ ($r^2 = 0.997$; SD = 7.59×10^{-3}).

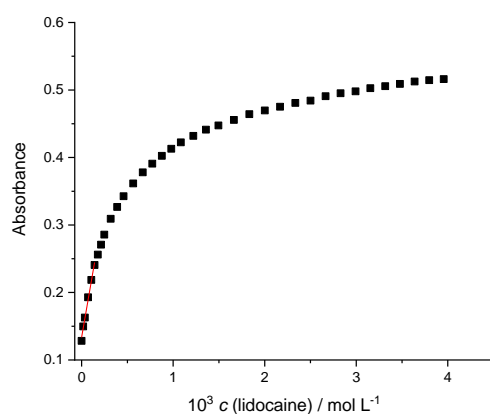


Figure S51. Curve for the titration of **3a** with lidocaine in water, utilized to estimate values of LOD and LOQ. Fitting of experimental data (—), LOD = $5.72 \times 10^{-6} \text{ mol L}^{-1}$, and LOQ = $1.75 \times 10^{-5} \text{ mol L}^{-1}$ ($r^2 = 0.998$; SD = 3.81×10^{-3}).

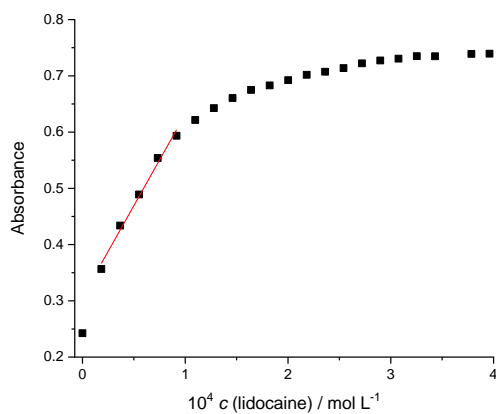


Figure S52. Curve for the titration of **4a** with lidocaine in water, utilized to estimate values of LOD and LOQ. Fitting of experimental data (—), LOD = $3.57 \times 10^{-6} \text{ mol L}^{-1}$, and LOQ = $1.19 \times 10^{-5} \text{ mol L}^{-1}$ ($r^2 = 0.989$; SD = 1.16×10^{-2}).

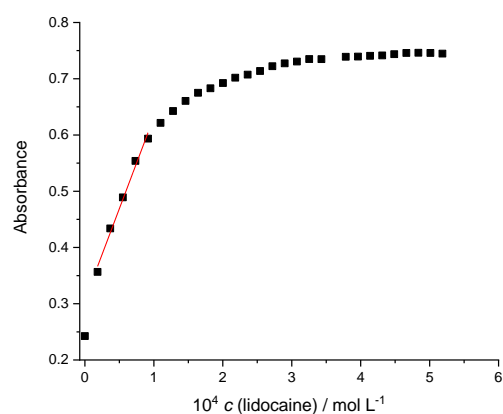


Figure S53. Curve for the titration of **3a** with lidocaine in water containing CTAB ($1.0 \times 10^{-3} \text{ mol L}^{-1}$), utilized to estimate values of LOD and LOQ. Fitting of experimental data (—), LOD = $5.35 \times 10^{-6} \text{ mol L}^{-1}$, and LOQ = $1.78 \times 10^{-6} \text{ mol L}^{-1}$ ($r^2 = 0.994$; SD = 1.58×10^{-2}).

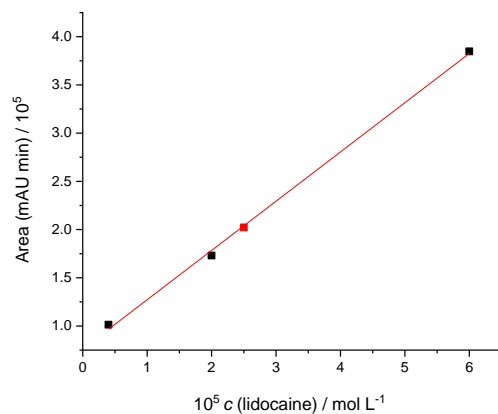


Figure S54. Calibration curve for standard (■) and commercial (■) lidocaine using LC-MS technique. A Phenomenex C18 column (particle size = $5 \mu\text{m}$; internal diameter = 4.6 mm ; length = 150 mm) was utilized. The experiments were performed in acetonitrile, the volume injection was of $10 \mu\text{L}$ and the flow rate was 0.2 mL min^{-1} .

Datafile Name:AM05_Solvente.lcd
Sample Name:AM05_Lidocaina_Comercial
Sample ID:Alberton

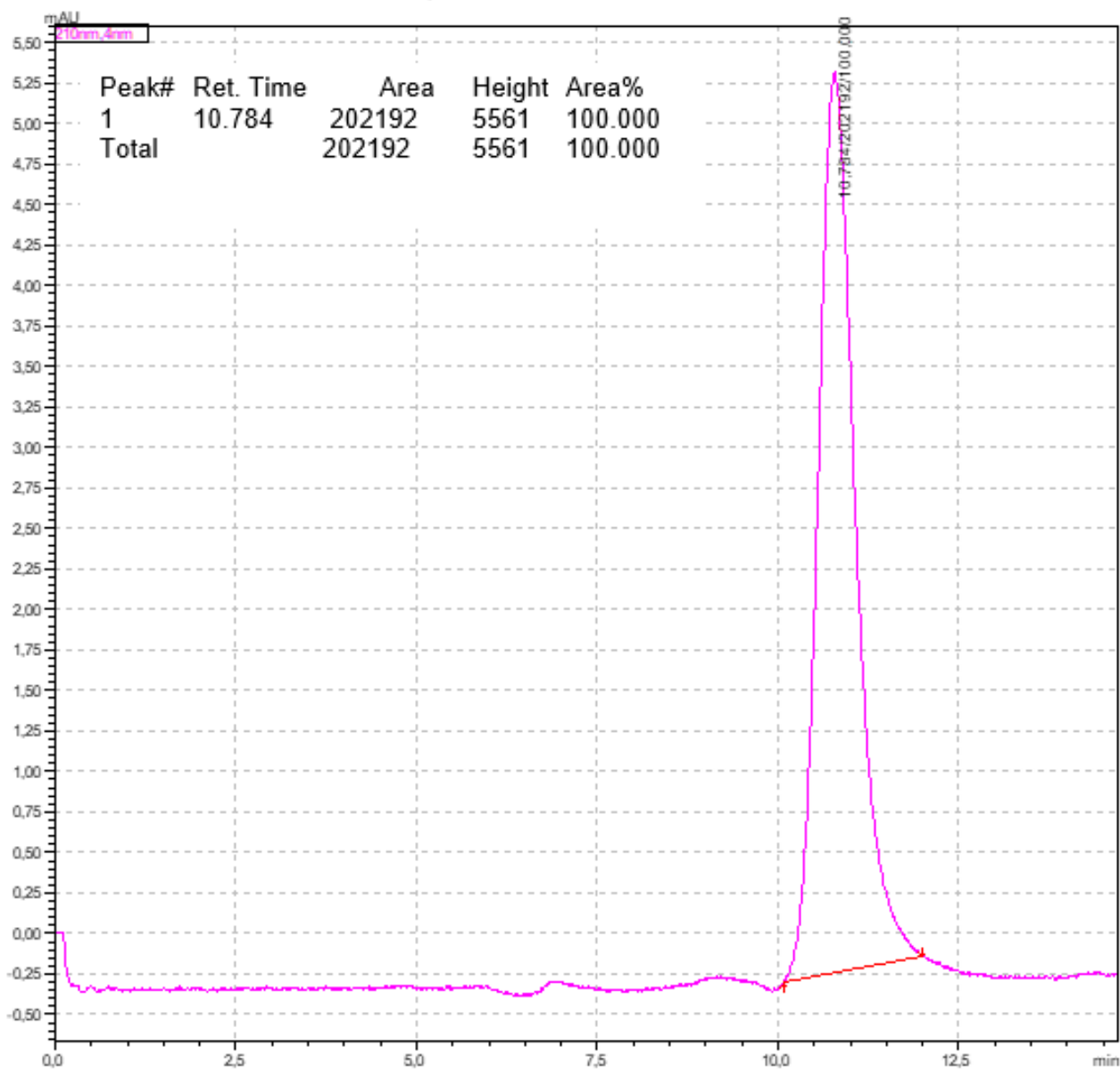


Figure S55. Chromatogram of the commercial lidocaine ($c(\text{lidocaine}) = 2.5 \times 10^{-5} \text{ mol L}^{-1}$).

Datafile Name: AM07_Lidocaina_Padrão_Farmacéutico.lcd
Sample Name: AM07_Lidocaina_Padrão_Farmacéutico
Sample ID: Alberton

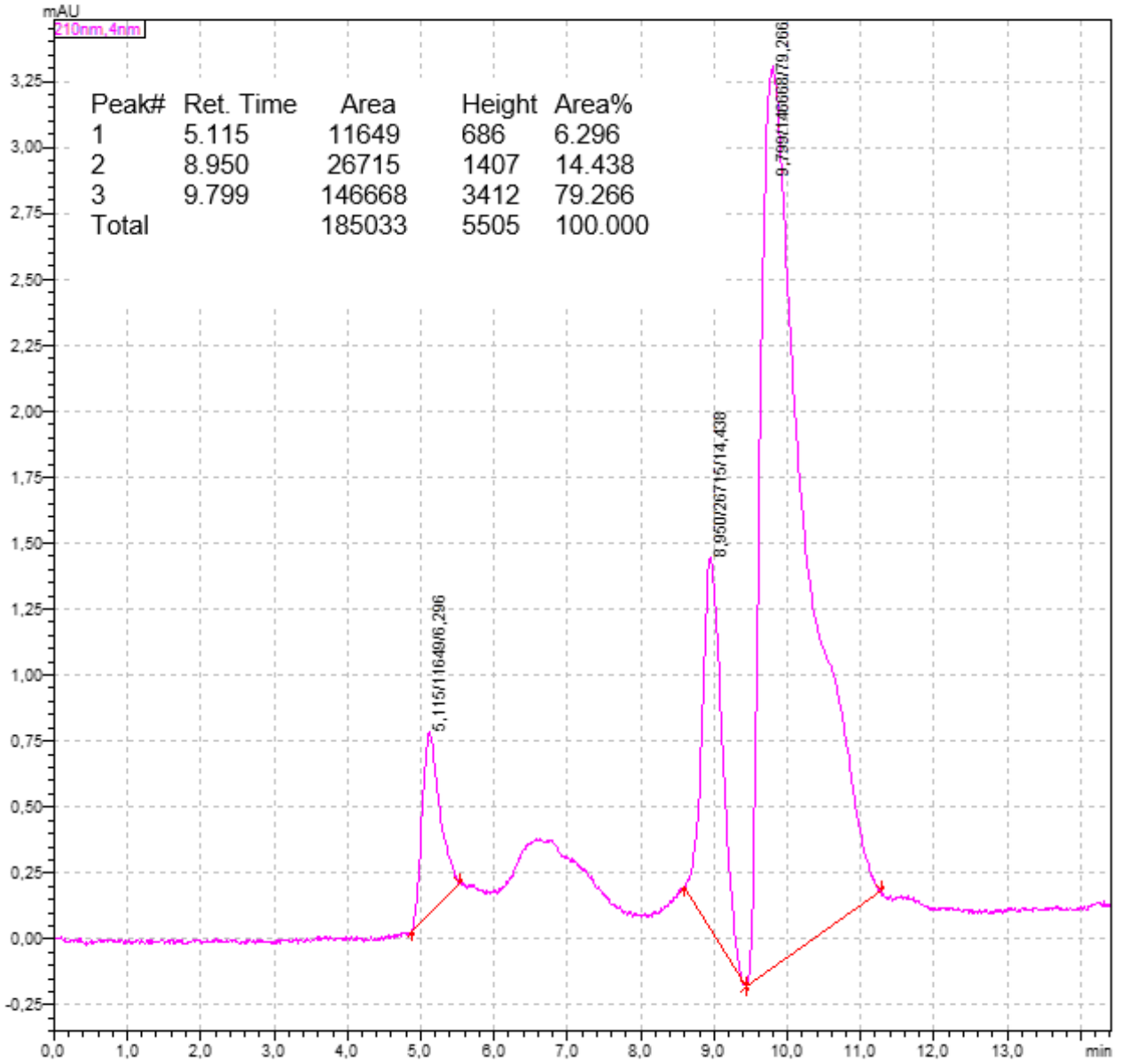


Figure S56. Chromatogram of the standard lidocaine ($c(\text{lidocaine}) = 3.9 \times 10^{-6} \text{ mol L}^{-1}$).

Datafile Name:AM09_Lidocaina_Padrão_Farmacêutico.lcd
Sample Name:AM09_Lidocaina_Padrão_Farmacêutico
Sample ID:Alberton

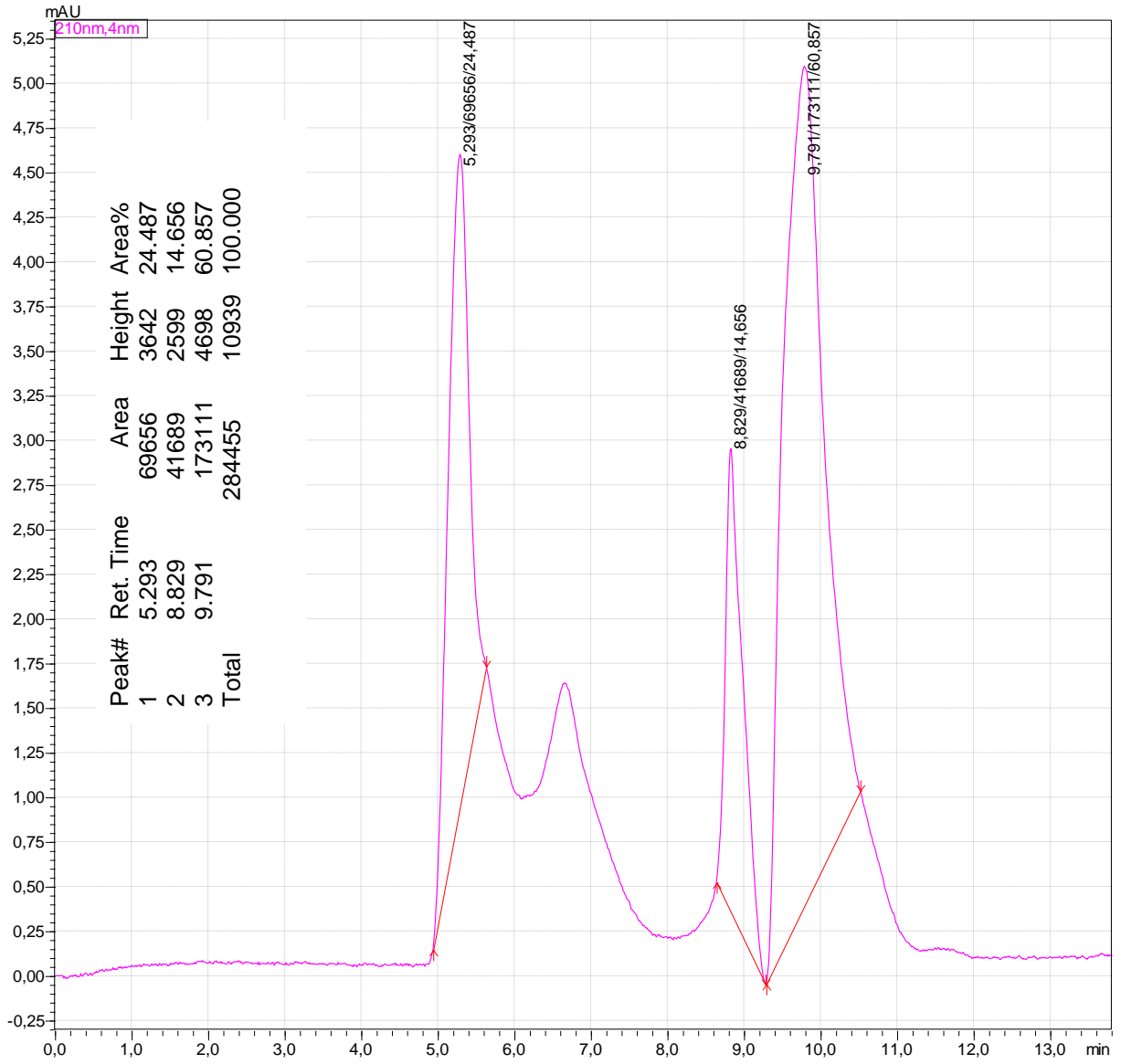


Figure S57. Chromatogram of the standard lidocaine ($c(\text{lidocaine}) = 1.9 \times 10^{-5} \text{ mol L}^{-1}$).

Datafile Name: AM010_Lidocaina_Padrão_Farmacéutico.lcd
Sample Name: AM010_Lidocaina_Padrão_Farmacéutico
Sample ID: Alberton

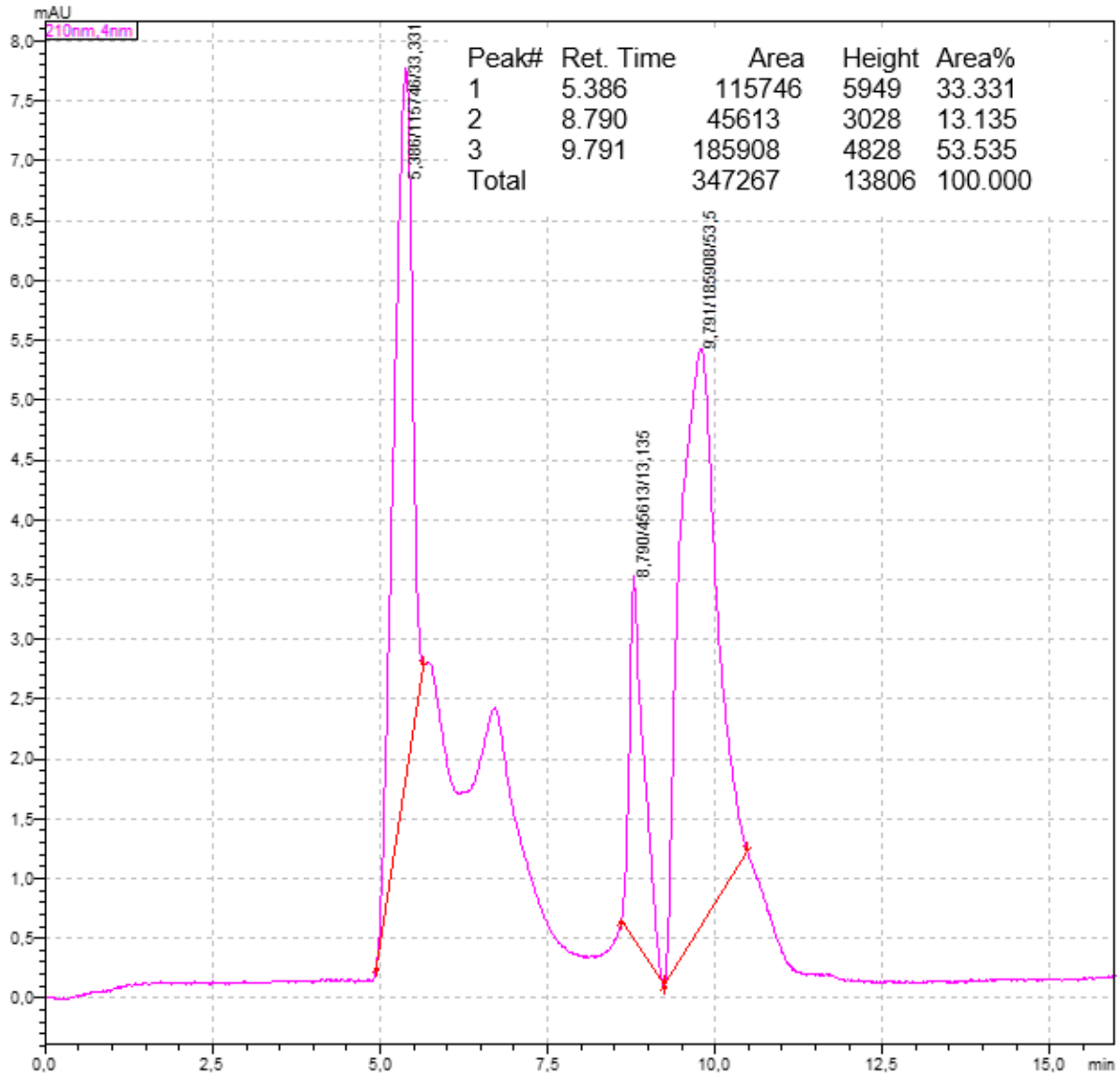


Figure S58. Chromatogram of the standard lidocaine ($c(\text{lidocaine}) = 6.0 \times 10^{-5} \text{ mol L}^{-1}$).

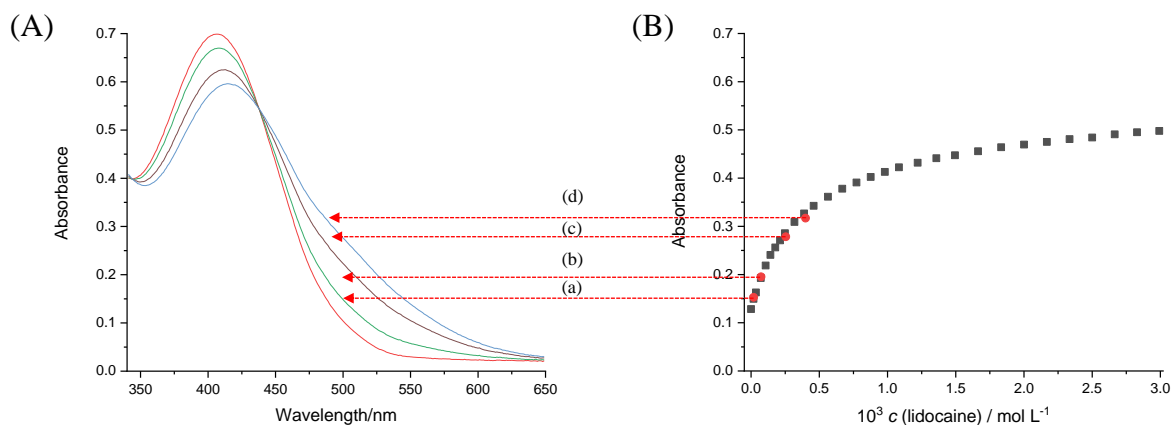


Figure S59. (A) UV-Vis spectra of **3a** in water without amine (a) and with (b) 1.45×10^{-4} , 2.54×10^{-4} (c), and (d) $3.99 \times 10^{-4} \text{ mol L}^{-1}$ of a commercial sample of lidocaine. (B) Curve at 490 nm for the titration of compound ($4.0 \times 10^{-5} \text{ mol L}^{-1}$) with increasing amounts of a standard pharmaceutical lidocaine in 490 nm. The red circles correspond to the commercial samples of lidocaine.

References

1. Juranić, I.; *Croat. Chem. Acta* **2014**, *87*, 343.
2. Gohar, G. A.; Habib, M. M.; *Spectrosc. Int. J.* **2000**, *14*, 99.

